Evaluation of the global aerosol microphysical ModelE2-TOMAS model against satellite and ground-based observations

Y. H. Lee[1], P. J. Adams[2], and D. T. Shindell[1]
[1] Earth and Ocean Sciences, Nicholas School of the Environment, Duke University, Durham, NC 27708
[2] Department of Civil and Environmental Engineering and Department of Engineering Public Policy, Carnegie Mellon University, Pittsburgh, PA USA

Corresponding author: Y. H. Lee (yunha.lee.00@gmail.com)

Abstract

The TwO-Moment Aerosol Sectional microphysics model (TOMAS) has been integrated into the state-of-the-art general circulation model, GISS ModelE2. This paper provides a detailed description of the ModelE2-TOMAS model and evaluates the model against various observations including aerosol precursor gas concentrations, aerosol mass and number concentrations, and aerosol optical depths. Additionally, global budgets in ModelE2-TOMAS are compared with those of other global aerosol models, and the ModelE2-TOMAS model is compared to the default aerosol model in ModelE2, which is a One-Moment Aerosol (OMA) model (i.e., no aerosol microphysics). Overall, the ModelE2-TOMAS predictions are within the range of other global aerosol model predictions, and the model has a reasonable agreement (mostly within a factor of two) with observations of sulphur species and other aerosol components as well as aerosol optical depth. However, ModelE2-TOMAS (as well as ModelE2-OMA) cannot capture the observed vertical distribution of sulphur dioxide over the Pacific Ocean possibly due to overly strong convective transport and overpredicted precipitation. The ModelE2-TOMAS model simulates observed aerosol number concentrations and cloud condensation nuclei concentrations roughly within a factor of two. Anthropogenic aerosol burdens in ModelE2-OMA differ from ModelE2-TOMAS by a few percent to a factor of 2 regionally, mainly due to differences in aerosol processes including deposition, cloud processing, and emission parameterizations. We observed larger differences for naturally emitted aerosols such as sea salt and mineral dust, as those emission rates are quite different due to different upper size cutoff assumptions.

1. Introduction

Aerosols perturb the energy balance of the Earth-atmosphere system by scattering and absorbing solar and terrestrial radiation, known as the aerosol direct effect, and by modifying cloud properties by acting as cloud condensation nuclei (CCN), known as

aerosol indirect effects (e.g. Lohmann and Feichter, 2005; Forster and Ramaswamy, 2007). The recently published IPCC AR5 (Intergovernmental Panel on Climate Change Fifth Assessment Report) refers to these as aerosol-radiation interactions and aerosol-cloud interactions, respectively (Boucher et al., 2013). For light-absorbing aerosols such as black carbon and mineral dust, the ambient air can be heated as a result of their direct effect, affecting relative humidity and atmospheric stability, which is known as the semi-direct effect. The largest uncertainty in estimating anthropogenic climate forcing is from the aerosol indirect effects (Myhre et al., 2013b). Since it is not easily estimated from observations due to natural variability in cloud properties and the lack of observations of the pre-industrial atmosphere, estimates of aerosol indirect forcing have been mainly based on general circulation models (GCMs). Thus, there have been growing efforts to develop and improve aerosol microphysics models for a more physically based representation of atmospheric aerosol number and CCN concentrations (e.g. Adams and Seinfeld, 2002; Easter et al., 2004; Vignati et al., 2004; Lauer et al., 2005; Liu et al., 2005; Spracklen et al., 2005; Stier et al., 2005; Bauer et al., 2008; Trivitayanurak et al., 2008; Yu and Luo, 2009; Mann et al., 2010; Lee and Adams, 2012).

Aerosol microphysics models can be broadly categorized into modal and sectional methods, depending on how they represent the aerosol size distribution. In general, modal-based methods use an analytical function (e.g. a lognormal distribution) to represent a subset of the particle population. Sectional methods represent a size distribution by predicting aerosols in several size sections or "bins". Additionally, sectional and modal methods may differ from each other in numerous ways, including the number of moments of the size distributions that are tracked in each section or mode.

Sectional methods can be divided into single-moment sectional methods that typically track either aerosol number or mass in each bin and two-moment sectional methods that explicitly track both aerosol number (i.e. 0^{th} moment) and mass (i.e. 1^{st} mass moment or 3^{rd} radial moment) in each size section. Unlike single-moment sectional approaches, two-moment sectional methods can conserve both number and mass very accurately (Tzivion et al., 1987; Feingold et al., 1988; Harrington and Kreidenweis, 1998; Tzivion et al., 2001; Adams and Seinfeld, 2002; Jung et al., 2006) but have a high computational burden. The modal approaches are generally more computationally

efficient but may not represent abrupt transitions in a size distribution well, which can occur during cloud processing (Zhang et al., 1999).

The TOMAS aerosol microphysics model (Adams and Seinfeld, 2002; Tzivion et al., 1987;Tzivion et al., 1989) has been developed to study tropospheric aerosol microphysics and predict cloud condensation nuclei (CCN) concentrations. The TOMAS model has been previously implemented into the climate model of Goddard Institute for Space Studies General Circulation Model II-prime (GISS GCM II-prime), referred to as "GISS-TOMAS" (Lee and Adams, 2010). It has also been incorporated into GEOS-CHEM (Trivitayanurak et al. 2008), the regional model PMCAMx-UF (Jung et al., 2010), and the Large-Eddy Simulation model (Stevens et al., 2012;Singh et al., 2014). The GISS GCM II-prime has horizontal grid dimensions of 4˚ latitude and 5˚ longitude, with nine vertical sigma layers between the surface and the 10 hPa level (Hansen et al., 1983). Modules for each of the major aerosol species have been developed for the GISS GCM II-prime, and the GISS-TOMAS model has been evaluated with ground-level measurements such as number and mass concentrations, deposition fluxes, and remote sensing observations (Adams and Seinfeld, 2002; Pierce and Adams, 2006; Pierce et al., 2007; Lee et al., 2009; Lee and Adams, 2010). Despite the accuracy in predicting aerosol microphysical process in TOMAS, the original version of TOMAS has a heavy computational burden. Lee and Adams (2012) developed less computationally expensive configurations of the TOMAS model (Fast TOMAS), which are 2-3 times faster than the original TOMAS model with only a few percent increases in microphysical errors. However, a remaining weakness for the GISS-TOMAS model is the outdated host model, the GISS GCM II-prime.

Here, we incorporate the TOMAS model into the new version of GISS GCM (i.e., ModelE2), referred to as "ModelE2-TOMAS". ModelE2 now has three different aerosol models available: TOMAS, the One-Moment Aerosol model (hereafter, referred to as OMA) (e.g. Koch et al., 2006) that has no microphysics, and the modal-based aerosol microphysics model, MATRIX (Multiconfiguration Aerosol TRacker of mIXing state) (Bauer et al., 2008). The combination of several aerosol models allows ModelE2 to explore the uncertainties in predicting aerosol characteristics and their climate effects that are associated with aerosol modelling (e.g. different numerical approaches) in the same

host model. We also note that it was important to implement the TOMAS aerosol model into the ModelE2 host model because uncertainties in the estimates of aerosol forcing come not only from aerosol modelling itself but also other parts of the host GCM (e.g., cloud physics, planetary boundary layer, and advection).

ModelE2-TOMAS has been used in several recent studies under the Atmospheric Chemistry and Climate Model Intercomparison Project (ACCMIP) which aims to understand composition changes and the associated radiative forcing between 1850 and 2100 (Bowman et al., 2013; Lamarque et al., 2013a; Lamarque et al., 2013b; Lee et al., 2013a; Nabat et al., 2013; Naik et al., 2013; Shindell et al., 2013; Stevenson et al., 2013; Young et al., 2013). Here we give a detailed description of ModelE2-TOMAS and evaluate against ModelE2-OMA (e.g., Schmidt et al., 2014) and observations of aerosol mass and number as well as aerosol optical depth. Section 2 and 3 provide descriptions of ModelE2-OMA and ModelE2-TOMAS, respectively. Section 4 explains the emissions and design of the simulations. Section 5 presents global budgets of the simulated aerosols and the evaluation of the ModelE2-TOMAS and ModelE2-OMA against observations of aerosol mass concentrations and aerosol optical depth and the evaluation of the TOMAS number predictions against observations. Conclusions follow in Section 6. We note that aerosol direct and indirect forcings using ModelE2-TOMAS will be discussed in a separate paper.

2. GISS GCM ModelE2

In this section, we briefly describe ModelE2 (Schmidt et al. (2014)), the GISS climate model used to perform Coupled Model Intercomparison Phase 5 (CMIP5; Taylor et al, 2012). The model physics are mostly similar to GISS ModelE (CMIP3 version: Schmidt et al., 2006). The model has 2° latitude by 2.5° longitude resolution, with 40 vertical hybrid sigma layers from the surface to 0.1 hPa (80 km). Tracers, heat, and humidity are advected using the highly nondiffusive Quadratic Upstream Scheme (Prather, 1986). The radiation scheme accounts for size-dependent scattering properties of clouds and aerosols based on Mie scattering (Hansen et al., 1983) and non-spherical light scattering of cirrus and dust particles based on T-matrix theory (Mishchenko et al., 1996). It also includes the impact of water uptake by hygroscopic species on their radiative properties. In the model,

clouds are distinguished into convective and large-scale stratiform clouds. The clouds parameterizations are similar to Del Genio (1993) and Del Genio et al. (1996) but have been improved in several respects (see details in Schmidt et al., 2006; Schmidt et al., 2014). The physics timestep is 30 minutes, and the radiation is calculated every 2.5 hours.

2.1 ModelE2-OMA description

ModelE2 includes a default aerosol module, OMA (One-Moment Aerosol), which has no microphysics. ModelE2-OMA has sulphate (Koch et al., 2006; Koch et al., 2007; Koch et al., 2011), carbonaceous aerosols (Koch et al., 2007), secondary organic aerosols (Tsigaridis and Kanakidou, 2007), sea salt (Koch et al., 2006; Tsigaridis et al., 2013), dust (Miller et al., 2006), and nitrate (Bauer et al., 2007). Along with sulphate, the model also predicts sulphur dioxide, dimethyl sulfide (DMS) and methanesulfonic acid (MSA) (Koch et al., 2006). The secondary organic aerosol formation is computed using a two-product model with isoprene, monoterpenes, and sesquiterpenes as SOA precursors (described in Tsigaridis and Kanakidou, 2007). Sea salt particles have two size classes with a fine mode (0.1 μm to 1 μm in dry radii) and a coarse mode (1 μm to 4 μm in dry radii). Dust particles have four size classes with radii between 0.1-1 μm (clay), 1-2 μm (silt1), 2-4 μm (silt2), and 4-8 μm (silt3). The model accounts for heterogeneous chemistry on mineral dust particle surfaces to form nitrate and sulphate (Bauer and Koch, 2005).

In ModelE2, the surface boundary conditions are defined using dry deposition and interactive surface sources (Koch et al., 2006). The dry deposition scheme is tightly coupled to the model's boundary layer scheme and is based on a resistance-in-series scheme derived from the Harvard GISS-CTM, which is applied between the surface layer (10 m) and the ground (Koch et al., 2006). Wet deposition is determined by several processes including rainout within clouds, washout below precipitating regions, scavenging within and below cloud updrafts, evaporation of falling precipitation, transport along with convective plumes, and detrainment and evaporation from convective plumes (Koch et al., 2006; Shindell et al., 2006). ModelE2 includes a dissolved species budget scheme for stratiform clouds, which has an impact on sulphate

formation via aqueous oxidation, since some sulphate formed in clouds undergoes wet scavenging instead of being added back to the sulphate in air (Koch et al., 2006).

Tropospheric/stratospheric chemistry in ModelE2 includes 156 chemical reactions among 51 gas species (Shindell et al., 2013). In ModelE2, chemistry and aerosols are fully interactive, so that the oxidation fields used for sulphate formation are from the chemistry model (not prescribed) and the photolysis rates are affected by light attenuation by aerosols (Shindell et al., 2013). Photolysis rates are computed using the Fast-J2 scheme (Bian and Prather, 2002). Aerosol indirect effects are based on an empirical parameterization that compute cloud droplet number concentrations as a function of aerosol mass (Menon et al., 2002; Menon et al., 2008).

3. ModelE2-TOMAS description

The TOMAS aerosol microphysics model uses a sectional approach that represents the aerosol size distribution by predicting the amount of aerosol in several size categories or "bins". TOMAS tracks two moments of the aerosol size distribution in each size bin: total aerosol number (i.e., 0^{th} moment) and mass (i.e., 1^{st} mass moment). Total mass is decomposed into several aerosol species, allowing prediction of the size-resolved aerosol composition. In total, ten quantities are tracked for each size bin: sulphate mass, sea-salt mass, mass of pure (hydrophobic) elemental carbon (EC), mass of mixed (aged) EC, mass of hydrophobic organic matter (OM), mass of hydrophilic OM, mass of mineral dust, mass of ammonium, mass of water and the number of aerosol particles in that bin. In TOMAS, all ammonia becomes ammonium aerosol until sulfate is neutralized to form ammonium sulfate; the excess ammonia after neutralization remains as free gas-phase ammonia. The ammonium aerosol is partitioned into each size bin in proportion to the sulfate mass. However, ammonium is not size-resolved (i.e., bulk tracer) for the purpose of model processes outside of TOMAS such as advection and deposition. In addition, the model tracks four bulk gas-phase species: sulphur dioxide (SO_2), dimethylsulfide (DMS), sulphuric acid (H_2SO_4), and a lumped gas-phase tracer that represents oxidized organic vapours forming secondary organic aerosol (SOA). The gas-phase H_2SO_4 is assumed to be in pseudo-steady state equilibrium between its chemical production and condensational/nucleation losses (Pierce and Adams, 2009a). Water uptake by sulphate

and sea salt is based on a polynomial fit based on ISORROPIA, a thermodynamic equilibrium model for inorganic aerosols (Nenes et al., 1998). For water uptake by hydrophilic OM, it is based on the observations of Dick et al. (2000). The size section boundary is defined by dry particle mass, such that addition or removal of aerosol water mass does not move particles between sections. In general, TOMAS treats all aerosols as internally mixed during microphysics such as calculating condensation and coagulation rates. However, a portion of EC is treated as externally mixed for the purpose of wet deposition. A detailed description of the TOMAS microphysics scheme can be found in Adams and Seinfeld (2002), Lee and Adams (2012), and Lee et al. (2013b).

Several alternative nucleation schemes are available in TOMAS, including binary nucleation (Vehkamaki et al., 2002), ternary nucleation (Napari et al., 2002), ion-induced nucleation (Modgil et al., 2005), and activation nucleation with an A factor of 2×10^{-6} s^{-1} (Sihto et al., 2006) for the boundary layer (~up to 900 hPa). For the simulations used in this paper, only binary nucleation is used. The boundary-layer nucleation is off in all simulations because it tends to overpredict aerosol number concentrations in our model. Also we do not show any run with the ternary nucleation (Napari et al., 2002) because it overpredicts aerosol number concentration severely (not shown).

With Fast TOMAS models, the TOMAS microphysics module became more flexible in term of varying particle size resolution, i.e. the number of size bins (Lee and Adams, 2012). For the size range of 10 nm to 10 μm, the original TOMAS uses 30 bins (size boundary is defined with mass doubling), and the Fast TOMAS uses 15 bins or 12 bins (size boundary is defined with mass quadrupling). As discussed in Lee and Adams (2012), the Fast TOMAS reduces the computational burden by 2-3 times while generally predicting CCN concentrations within a few percent of the original TOMAS. The lower size cutoff in TOMAS can also vary from 10 nm to 3 nm or from 10 nm to 1 nm (Lee et al., 2013b). Among several possible configurations, ModelE2-TOMAS currently uses either 12 bins covering 10 nm to 10 μm or 15 bins covering 3 nm to 10 μm, which is the most computationally efficient version of TOMAS for the given size range. In this paper, we used TOMAS with 15 bins covering 3 nm to 10 μm (TOMAS15; see Table S1 in the supplementary materials): 3 bins cover from 3nm to 10 nm, 10 bins from 10 nm to 1 μm and the last two bins from 1 μm to 10 μm. The TOMAS15 version has become the

default model configuration for ModelE2-TOMAS, so we will refer to it as ModelE2-TOMAS throughout this paper. More configurations will be available in the near future.

The wet deposition scheme in ModelE2-TOMAS is identical to the one used in ModelE2-OMA except for the following. First, ModelE2-TOMAS adds sulphate mass produced in the aqueous phase directly to the bin-resolved sulphate mass in ambient air rather than maintaining a separate tracer for dissolved sulphate. Compared to ModelE2-OMA, this is a simplification because the sulphate formed in the aqueous phase will be only released as interstitial aerosol when the cloud water evaporates. It is adopted here for simplicity but will be improved in the future. The other difference is that the wet/dry deposition in ModelE2-TOMAS accounts for particle size dependence. For in-cloud scavenging, modified Köhler theory is used to obtain the critical supersaturation for activation of each size section and to determine which particles activate and are subject to in-cloud (nucleation) scavenging (Pierce et al., 2007). To determine activation, we assume kappa values of 0.7 for sulfate, 1.3 for sea-salt, and 0.15 for hydrophilic OM. The fraction of activated aerosols removed by wet deposition is proportional to the fraction of cloud water that precipitates, which is computed in each model layer. Wet deposition accounts for re-evaporation of precipitation. For in-cloud scavenging, the large-scale and convective clouds in the model are assumed to have a supersaturation of 0.2%; unlike GISS-TOMAS that used a supersaturation of 1.0% for convective clouds, a supersaturation of 0.2% is assumed in ModelE2-TOMAS in order to capture the observed Hoppel gap (~100 nm) in the marine boundary layer. Note that the activation described here to determine in-cloud scavenging is not used for computing cloud droplet number concentrations (see below). For below-cloud scavenging, a first-order removal scheme implemented for bulk aerosols by Koch et al. (1999) is modified for size-resolved aerosols (Adams and Seinfeld, 2002). Dry deposition is identical to the existing resistance-in-series scheme in ModelE2, but ModelE2-TOMAS considers size-dependent gravitational settling of particles and size-dependent resistance in the quasi-laminar sublayer (Seinfeld and Pandis, 1998; Adams and Seinfeld, 2002).

To compute the cloud microphysics properties as a function of aerosols (i.e., the aerosol-cloud interactions), ModelE2-TOMAS uses a physical-based activation parameterization from Nenes and Seinfeld (2002). A critical supersaturation is computed

in the parameterization using a model updraft velocity that is computed based on a large-scale vertical velocity and sub-grid velocity.

In ModelE2-TOMAS, Mie theory is used to compute size-resolved AOD. For each grid cell, particle compositions (including aerosol-water) in each individual size bin are used to compute the volume-averaged refractive index and optical properties based on Mie theory. The optical properties are used to compute aerosol optical depth taking into account the aerosol concentration.

ModelE2-TOMAS is coupled to the same gas chemistry model (Shindell et al., 2013) as ModelE2-OMA. So the oxidation fields used for sulphate formation are from the chemistry model. However, unlike ModelE2-OMA, the photolysis rates are not affected by aerosols.

4. Description of the simulations

4.1 Emissions

The emissions used in this study are summarized in Table 1. The simulations used year-2000 emissions from the anthropogenic emissions inventory created for CMIP5 (Lamarque et al., 2012) and climatologically averaged biomass burning emissions from GFED3 for 1997 to 2009 (van der Werf et al., 2010). For SO_2, in addition to the anthropogenic emissions, continuous volcanic emissions from GEIA (Global Emissions InitiAtive; Andres and Kasgnoc, 1998) are used but increased by a factor of 1.5 as in the AEROCOM intercomparison emissions in Dentener et al. (2006). Sea-salt emissions are based on Gong (2003), which extends the lower size limit of the Monahan et al. (1986) emission from 0.4 μm to 0.02 μm. Dust emissions are based on the source distribution from Ginoux et al. (2001) and are proportional to the third power of the wind speed (at 10 m in height) above a threshold that is a function of soil moisture. Subgrid-scale variation of the wind speed in a GCM grid box, which is created by boundary-layer turbulence and dry/wet convection, is accounted for in the modelled dust emissions (Cakmur et al., 2006; Miller et al., 2006). DMS emissions are based on the seawater DMS concentrations of Kettle et al. (1999). For the sea-to-air transfer function used in the DMS emissions, the

ModelE2-TOMAS runs are based on Liss and Merlivat (1986), and the ModelE2-OMA model run is based on Nightingale et al. (2000).

Nightingale et al. (2000) provides a revised parameterization based on observations of the sea-to-air transfer rate scatter between two classical parameterizations (i.e., Liss and Merlivat, 1986;Wanninkhof, 1992), and it has been more favoured in many global DMS models than the two classical parameterizations. However, DMS emissions are quite uncertain. Estimates of the global DMS emissions range from 16 to 54 Tg S yr^{-1} (Kettle and Andreae, 2000), depending on the choice of DMS sea surface climatology, sea-to-air transfer rate parameterization, and wind speed data. DMS emission rates from ModelE2-TOMAS (16.1 Tg S yr^{-1}; see Table 3) and ModelE2-OMA (28.7 Tg S yr^{-1}; see Table 3) are within this range. The Liss and Merlivat (1986) parameterization is used in ModelE2-TOMAS, because a ModelE2-TOMAS run based on Nightingale et al. (2000) overpredicts the SO_2 concentrations over remote oceanic regions especially in the southern hemisphere. Koch et al. (2006) showed that the sea-to-air transfer function from Nightingale et al. (2000) increased annual DMS emissions by roughly a factor of two compared to the emission based on Liss and Merlivat (1986). This was desirable in ModelE2-OMA because of the underprediction of sulphate in remote oceanic regions in that model, although the model DMS and MSA (oxidized from DMS) tended to be excessive in SH oceanic regions especially near Antarctica. However, despite the higher DMS emissions, it turned out that the sulphate was still underpredicted because sulphate formed by aqueous oxidation was subject to wet scavenging before releasing to the ambient air as a result of the updated dissolved species budget scheme (Koch et al., 2006).

4.2 ModelE2-TOMAS run setup

We performed the simulations nudged with winds from the MERRA (Modern Era Retrospective-analysis for Research and Applications; Rienecker et al., 2011) reanalysis meteorological fields from 2000 to 2003 with 3 years spin-up (i.e., 1997-1999). Primary emissions of particulate sulphate are assumed to be 1.0 percent of total sulphur emissions. Emissions size distributions assumed for ModelE2-TOMAS are summarized in Table 2. Primary sulphate emissions are assumed to have a bi-modal lognormal distribution that

assigns 5% of the primary sulphate emissions as a nucleation mode with a geometric number mean diameter (GMD) of 10 nm and a geometric standard deviation (GSD) of 1.6 and the rest as an Aitken mode with GMD of 70 nm and GSD of 2. For fossil fuel and biofuel emissions, the size of primary carbonaceous aerosol emissions are assumed to follow a lognormal size distribution with a GMD of 60 nm and a GSD of 1.59 for both EC and OM (Stier et al., 2005). For carbonaceous aerosols of biomass burning emissions, a lognormal size distribution is assumed to have a GMD of 150 nm and a GSD of 1.59. Note that although the emission size distribution for biofuel emissions is generally assumed to be the same as that for biomass burning emissions (e.g. Dentener et al., 2006), in ModelE2-TOMAS run, we assumes the biofuel emission size distributions follow the finer fossil fuel size settings because the CMIP5 emissions does not provide a separate category for biofuel emissions (e.g. biofuel used for cooking and heating are assigned as the residential sector, which also includes fossil fuel usage). The OC (organic carbon): OM (organic matter) ratio is assumed to be 1:1.4.

ModelE2-TOMAS assumes larger particles for primary sulphate and carbonaceous aerosols than GISS-TOMAS (e.g., Lee et al., 2013b) to capture the observed aerosol number concentrations better. This is very likely due to the following: 1) GISS-TOMAS attributed the primary sulphate emissions only to anthropogenic sulphur emissions (excluding biomass burning emissions), while ModelE2-TOMAS attributes these to all sulphur emissions; 2) GISS-TOMAS applied the biomass-burning emission size distributions of carbonaceous aerosols to the biofuel emissions, which is coarser than the fossil fuel emission size distribution. Note also that the emission size distributions used for biomass burning and volcanic emissions are finer than the AEROCOM recommendations in Dentener et al. (2006). However, the model number concentrations and size distributions are changed little when applying the AEROCOM recommended emission distributions (not shown). Note that the biomass burning and volcanic emissions for sulphur are 1.4 Tg S $yr^{-1}$and 12.5 Tg S yr^{-1}, respectively.

Following the soil size assumptions used in GISS-TOMAS (Lee et al., 2009), the clay distribution is assumed to have a GMD of 0.14 μm and a GSD of 2, and the silt distribution, a GMD of 1.15 μm and a GSD of 2. Using this distribution, fifteen percent

of the silt emissions flux falls out of the upper size cutoff (i.e., 10 μm), and is therefore not received by any of the TOMAS size bins.

Compared to the run setup described above (hereafter, referred to as the "BASE" run), we additionally ran two other sensitivity runs with the ModelE2-TOMAS model by perturbing the nucleation process to evaluate changes in number concentrations (Table 1). The first sensitivity run is called "NoNUC", in which we turned off nucleation to estimate the contribution of primary emissions to aerosol number concentrations. The other run is called "LowNUC", in which we reduced the nucleation rate by using 5 times lower sulphuric acid concentrations to compute nucleation rates. Note that sulphuric acid concentrations are not perturbed in other processes, and the model sulphuric acid budget is little influenced by this treatment.

4.3 ModelE2-OMA run setup

To compare to the ModelE2-TOMAS run, we also ran the ModelE2-OMA model nudged to the same MERRA reanalysis meteorology with 3 years spin-up. However, the natural emissions and associated settings are not always the same between the two models because we chose to maintain the natural emissions/setup used in ModelE2-OMA, which has been chosen carefully in previous studies. To assist the interpretation of the results, we briefly summarize the differences between ModelE2-OMA and ModelE2-TOMAS. First, as mentioned in Section 4.1, the ModelE2-OMA model uses the sea-to-air transfer function of Nightingale et al. (2000) instead of Liss and Merlivat (1986), because Koch et al. (2006) argues that the newer DMS emissions improve sulphate predictions in the remote marine locations. Second, the same sea salt and dust emission schemes are applied in both aerosol models, but different assumptions for the upper limit of particle size are used: 8 μm in diameter for sea salt and 16 μm in diameter for dust in the ModelE2-OMA model; 10 μm in diameter for all species in ModelE2-TOMAS. Third, the ModelE2-OMA model assumes 2.5% of the total sulphur as primary sulphate as followed by the AEROCOM study (Dentener et al., 2006) whereas ModelE2-TOMAS assumes only 1%. Aerosol number predictions are sensitive to the primary sulphate assumption, but sulphate mass concentrations are not. When using the 2.5% assumption in ModelE2-TOMAS, we found that the simulated aerosol number

concentrations were biased high, and the model size distribution predictions were also poor. Note that Pierce and Adams (2009b) shows that GISS-TOMAS also overpredicts aerosol number concentration with the 2.5% assumptions.

5. Model results and evaluation

In this section, we present global-annual budgets, spatial distributions, and evaluations of the model aerosol precursor gases (in Sect. 5.1), aerosol mass (in Sect. 5.2 and 5.3), aerosol optical depths (AODs; in Sect. 5.4) and aerosol number (in Sect. 5.5 and 5.6). The observations used for model evaluations are from surface-based, aircraft-based and remote-sensing measurements. More details of the observations are provided in each subsection. To compare with the ModelE2-TOMAS results, we included the ModelE2-OMA results in global-annual budgets and model evaluations. Only the BASE run results are used in Section 5.1 to 5.4 because the predicted aerosol precursor gases concentrations, aerosol mass concentrations, and AODs from the nucleation sensitivity runs are quite similar to the BASE run.

Model skill is quantified in terms of log-mean normalized bias (LMNB) and log-mean normalized error (LMNE) when evaluating with annual-mean concentrations measurements and normalized mean bias (NMB) and correlation coefficient (R) when evaluating with an observed annual cycle and aerosol optical depth (both monthly and annually averaged AODs).

5.1 Aerosol precursor gases

Global budgets of DMS and SO_2 in ModelE2-TOMAS are presented in Table 3 with a range obtained from several global models including Wang et al. (2011), Liu et al. (2005), and those listed in Liu et al. (2005). The DMS and SO_2 budgets in ModelE2-TOMAS are within the ranges of the other global models. In the case of ModelE2-OMA (in Table 3), the global burden of DMS is about a factor of two higher than the ModelE2-TOMAS model because the DMS emission rate is ~78% higher by using the sea-to-air transfer functions by Nightingale et al. (2000). Despite the different DMS emissions and SO_2 emissions (due to the primary sulphate emission assumption, 1% versus 2.5%), the

global burden of SO_2 is quite similar to that in the ModelE2-TOMAS model. The dominant SO_2 removal processes are aqueous oxidation and dry deposition in both simulations. Boucher et al. (2003) simulates atmospheric DMS in the LMD-ZT model using the same DMS emission schemes as ModelE2-OMA (i.e., EXP1 in their study) and ModelE2-TOMAS (i.e., EXP4 in their study). The global DMS budgets from ModelE2-OMA and ModelE2-TOMAS agree quite well with the EXP1 (within 25 %) and EXP4 (within 15%).

When using the same DMS emissions in ModelE2-TOMAS as in ModelE2-OMA, the DMS global budgets are almost identical, but the SO_2 budgets vary substantially due to the differences in SO_2 modelling, i.e., heterogeneous SO_2 oxidation and photolysis (see Section 2). The heterogeneous sulphur dioxide oxidation on dust aerosol surfaces, which is only included in ModelE2-OMA, accounts for 25% of the total gas-phase oxidation loss. Based on Bauer and Koch (2005), including the heterogeneous chemistry, global SO_2 burden can decrease by 32%, and the global sulphate burden can increase by 3%. The simulated photolysis rates in ModelE2-OMA are affected by aerosol optical depth, affecting hydroxyl (OH) and other gas tracer concentrations - Naik et al. (2013) show a higher OH concentration in ModelE2-TOMAS than ModelE2-OMA. Overall, using the same DMS emissions in ModelE2-TOMAS results in a higher SO_2 burden and worse agreement for SO_2 and sulphate concentrations over remote oceanic regions (not shown).

The global budgets of H_2SO_4 and SOA precursor gas in the ModelE2-TOMAS model are not included in Table 3 but are summarized here. The simulated H_2SO_4 has a total production rate of 12.3 Tg S yr^{-1}, matching the SO_2 gas-phase oxidation, and is used in aerosol microphysics (i.e. 12 Tg yr^{-1} for condensation and 0.3 Tg yr^{-1} for nucleation). The model SOA precursor gas has a total production rate of 17.1 Tg yr^{-1}, assumed to be 10% of the terpene emission, and is condensed as hydrophilic OM. For ModelE2-OMA, the total production rate of SOA is 14.6 Tg yr^{-1}. This is quite comparable to ModelE2-TOMAS, which treats SOA much more simply and has a production rate of 17.1 Tg yr^{-1}. The global burden of SOA in ModelE2-OMA is 0.6 Tg yr^{-1}.

Figure 1 shows global maps of annual-mean DMS and SO_2 column mass concentrations. The spatial distribution of DMS concentrations shown in Fig. 1a is driven by its emission and interactive OH and NO_3 concentrations, which oxidize DMS to form

MSA and SO_2. The model DMS concentrations are most pronounced in the Southern Ocean and the Northern Atlantic oceans due to high seawater DMS concentrations during summer. The simulated SO_2 concentration shown in Fig. 1b is very high over industrial regions due to the anthropogenic emissions and is also high over the Southern Ocean due to DMS oxidation. Several local hotspots of SO_2 shown in Fig. 1b are due to volcanic emissions.

Annually averaged surface-layer SO_2 concentrations from both ModelE2-TOMAS and ModelE2-OMA are evaluated against observations from the EMEP (European Monitoring and Evaluation Programme, http://www.emep.int) and CASTNET (Clean Air Status and Trends Network, http://epa.gov/castnet/javaweb/index.html) networks (see Fig. 2). We used 2000-2004 mean SO_2 measurements for the EMEP network and 1995-2005 mean SO_2 data for the CASTNET network. Performance of ModelE2-TOMAS and ModelE2-OMA for predicted SO_2 concentrations in these locations is almost the same (i.e. LMNB=0.25-0.26 and LMNE=0.34 for the EMEP network; LMNB=0.09 and LMNE=0.29 for the CASTNET network), and the continental SO_2 predictions agree with the observation on average roughly within a factor of two. The two aerosol models are almost the same because the anthropogenic emissions, which are identical in both models, are dominant at these locations.

Figure 3 compares surface-layer SO_2 and DMS mixing ratios from the two aerosol models against observations at three Southern Hemisphere remote sites: Amsterdam Island (DMS from Sciare et al., 2000; SO_2 from Nguyen et al., 1992), Cape Grim (Ayers et al., 1995), and Dumont (Jourdain and Legrand, 2001). Note that Dumont has only DMS measurements. For DMS, both models capture the observed seasonal cycle (i.e. $R>0.8$) generally well but are less successful over Dumont. The DMS concentrations seem to agree well against the observations when using the sea-air transfer function of Liss and Merlivat (1986), i.e., the case for ModelE2-TOMAS, but this run underpredicts during winter season at the Amsterdam Island site (in Fig. 3a) and during all season at Dumont site (in Fig. 3c). Earlier, we mentioned that the global DMS budgets from Boucher et al. (2003) agree well with those from ModelE2 when using the same DMS emission parameterization. However, Boucher et al. (2003) shows the better agreement to the same DMS measurements when using the sea-air transfer function of Nightingale et

al. (2000) at Amsterdam Island and Cape Grim (i.e., the case for ModeleE2-OMA), because their DMS mixing ratios from that simulations are actually more close to ModelE2-TOMAS. This may suggest that, at least over SH high latitude regions, the surface wind speed in ModelE2 is much stronger than that in LMD-ZT, resulting in higher DMS emissions and burden. We need to investigate further to find out a source for the difference though.

The ModelE2-TOMAS SO_2 shows very good agreement at Amsterdam Island but a high bias at Cape Grim (see Figs. 3d and e). We considered whether the overpredicted SO_2 in the model might be influenced by the emissions in the adjacent grids, which is mentioned in Mann et al. (2010), because the measured SO_2 at Cape Grim is filtered to include the marine sector only (Ayers et al., 1991). Sampling the model SO_2 from adjacent grids toward marine areas, the overprediction is reduced significantly (LMB is reduced from 10 to 3) but is still severe. The most plausible reason for the overprediction of SO_2 at Cape Grim might be the lack of SO_2 oxidation by ozone on sea salt particles, which is missing in our model. Korhonen et al. (2008) shows a reduction of SO_2 concentrations by a factor of 5 in January and a factor of 20 in July at Cape Grim when including SO_2 oxidation on sea spray particles, although their treatment of the reactions might overestimate the SO_2 oxidation rates.

Simulated DMS and SO_2 vertical profiles over the Pacific Ocean are compared against two sets of aircraft observations in Figures 4 and 5: PEM-Tropics-A performed during August-October, 1996 (Hoell et al., 1999) and PEM-Tropics-B during March-April, 1999 (Raper et al., 2001). Note that PEM-Tropics-A DC8 aircraft data is used and most of them were during September 1996, but model evaluation is little changed by comparing with model outputs in September or August-October average. The observed vertical profile data used here are binned into altitude ranges (Emmons et al., 2000). Model outputs are averaged over the observational time period and domain. Simulated DMS vertical profiles are very similar between the two aerosol models, although the surface DMS is different as their emissions are not the same. Both models show good agreement with the observations (mostly within 25^{th} and 75^{th} percentile of observed values), especially capturing a strong concentration decrease from the surface to the free troposphere.

In the case of SO_2, even though the agreement is not as good as that seen for DMS, both aerosol models seem to capture the observed magnitude approximately within a factor of two (see Fig. 5). The overall vertical patterns shown in the models are frequently not in agreement with the observations. Except at Hawaii, our model do not capture the enhanced SO_2 concentrations in the boundary layer shown in the observation, even though the model DMS is quite well captured. The poor prediction of SO_2 vertical profile might be due to 1) too much precipitation near tropics in ModelE2 (see Fig. 9 in Schmidt et al., 2014) and 2) too strong vertical transport (e.g., via deep convection over the tropical Pacific Ocean) in the model. The latter can be supported by that the small DMS peak at 8 km and the elevated SO_2 in the upper/free troposphere in the models (see Figs. 4 and 5),. Although the elevated SO_2 mixing ratios might be due to wet scavenging (including aqueous chemistry) of SO_2 being too weak, we did not see any noticeable improvement when increasing SO_2 Henry's law constant by a factor of two in the model (not shown). A large peak in the mid-troposphere at Hawaii in the models results from volcanic SO_2 emissions, while the observations show a similar peak only during March-April 1999, which is heavily influenced by volcanic emissions (Thornton et al., 1999). During August-October 1996, the observations at Tahiti and Easter Island show transport of volcanic SO_2 emissions in the middle and upper troposphere (Thorton et al., 1999), which is not captured in the model. Since our model includes only continuous volcanic emission with a yearly resolution, our model fails to simulate variability in volcanic SO_2 emissions at higher time resolution.

5.2 Aerosol mass budgets and distributions

Globally and annually averaged budgets of aerosols in the ModelE2-TOMAS model are shown in Table 4. For the sulphate and EC budgets, we use the ACCMIP multi-model mean from Shindell et al. (2013) and Lee et al. (2013a), which is based on 8 ACCMIP models using the same AR5 emission scenario. Note that the biomass burning emission in this study is GFEDv3 inventory averaged from 1997 to 2009, while the ACCMIP models use GFEDv2 inventory averaged from 1997 to 2006. We do not compare with the AEROCOM phase 2 multi-model mean presented in Myhre et al. (2013a) because the aerosol budgets in Myhre et al. (2013) are for anthropogenic aerosols, which is defined as

the difference between the present-day run and pre-industrial run. For the lifetime and deposition rate coefficient budgets, we compare with the AEROCOM Phase 1 multi-model mean presented in Textor et al. (2006) –hereafter, referred to as AEROCOM Phase 1.

For sulphate, the ModelE2-TOMAS total source rate is lower than the ACCMIP mean (43.7 Tg yr^{-1} vs. 51.7 Tg S yr^{-1}), and the global burden is the same as the ACCMIP mean burden (0.67 Tg S) due to the slightly longer lifetime in the ModelE2-TOMAS model (5.7 days vs. 5.0 days). Note that the GISS-E2-R-TOMAS model used for ACCMIP is almost identical to ModelE2-TOMAS evaluated here except for the sulfate modelling. The sulphate and DMS emissions used in GISS-E2-R-TOMAS are identical to those used in ModelE2-OMA in this paper. For dry deposition coefficient (the inverse of the lifetime), ModelE2-TOMAS has a particularly small value. However, the longer overall sulphate lifetime is contributed by both dry and wet deposition, rather than dry deposition. When increasing the dry deposition coefficient to the AEROCOM Phase 1 mean alone, the overall lifetime is decreased from 5.6 days to 4.8 days. Doing the same for wet deposition with no change in the dry deposition, the overall lifetime decreases from 5.6 days to 4.5 days.. Wet deposition accounts for 98% of the total deposition in ModelE2-TOMAS, which is much higher than AEROCOM Phase 1, and convective clouds contribute 27% of the wet deposition.

Global-annual EC in ModelE2-TOMAS is 0.19 Tg, which is very comparable to the ACCMIP mean (0.16 Tg). Similar to sulphate, wet deposition contributes >95% of total deposition of EC, which is higher than other ACCMIP models (see Table 3 in Lee et al., 2013a), and 24% of wet deposition is by convective clouds. For EC and OM, their lifetimes are longer than the ACCMIP mean as well as AEROCOM Phase 1 means but still within the standard deviation. Despite smaller dry deposition coefficients for EC and OM compared to the AEROCOM mean, their wet deposition coefficients are quite comparable to the AEROCOM mean.

The global annual burden of sea salt and dust in ModelE2-TOMAS are 3.6 Tg and 9.1 Tg, respectively. For sea salt and dust, dry deposition is as important as wet deposition due to their large particle sizes, accounting for 68% and 52% of total deposition, respectively. Since the size coverage of sea salt and dust in our model do not necessarily

match with those in the AEROCOM Phase 1 models, we do not compare the lifetime and removal rate coefficients, which is strongly influenced by the upper size cutoff used in their emissions.

Despite the same host model and the same anthropogenic emission scenarios as the ModelE2-TOMAS model, the ModelE2-OMA model shows significantly different aerosol mass budgets (in Table 5), which must arise from using different deposition assumptions and other aerosol modelling treatments (see Section 2 for the details). Sulphate burden and lifetime in ModelE2-OMA is roughly half of that in ModelE2-TOMAS. The total source rate of SO_4 is about 20% higher than ModelE2-TOMAS and is close to the ACCMIP mean value. The ModelE2-OMA model has a shorter lifetime for EC, leading to ~40% lower burden compared to ModelE2-TOMAS. The OM burden is quite similar between two models. SOA formation rate is slightly different (14.6 Tg yr^{-1} for ModelE2-OMA and 17.1 Tg yr^{-1} for ModelE2-TOMAS), but the difference is only a small portion (about 3-4%) of the total OM source rate. The sea-salt emission rate is lower than that in ModelE2-TOMAS due to the maximum size cutoff of 8 μm assumed in sea-salt emission, but its burden is more than a factor of two higher. For dust particles, the emission rate is higher than that in ModelE2-TOMAS due to the coarser size cutoff in their emissions (i.e. up to 16 μm), and the burden is higher. For sea salt, the contribution of wet deposition to total deposition is more than 2 times higher than that in ModelE2-TOMAS. Unlike ModelE2-TOMAS, ModelE2-OMA has nitrate aerosol, which has a global burden of 1.6 Tg with a lifetime of 6.4 days.

The removal rate coefficient of dry deposition is about 50-60 times higher for sulphate, EC and OM in ModelE2-OMA, making it more comparable to the AEROCOM mean values. The lower dry deposition rates with the ModelE2-TOMAS model is likely due to the size-dependent dry deposition parameterization. The dry deposition velocity is not saved in the ModelE2 output currently, so alternatively we refer to the Figure 1 in Adams and Seinfeld (2001) that presents the global and annual-average of size-resolved dry deposition velocities in GISS-TOMAS (sulphate alone) compared to the size-independent one. Although the dry deposition velocities from ModelE2-TOMAS might not be exactly the same as the ones in the model version used in Adams and Seinfeld (2001) due to the updates made in ModelE2 (e.g. the boundary layer module), this point

should be valid because the dry deposition parameterizations in both models have been little changed. Despite the large differences in dry deposition rates for accumulation mode particles, dry deposition is a fairly minor removal pathway in both models.

Figure 6 shows simulated global distributions of annual-mean concentrations of ModelE2-TOMAS sulphate, EC, OM, sea salt and dust in the lowermost layer. The sulphate concentrations are high over industrial regions, driven by the SO_2 emissions and OH/H_2O_2 oxidant concentrations. Simulated EC and OM concentrations are high over the biomass burning regions and the industrial regions, especially East Asia and South Asia, but the OM concentrations are particularly pronounced over biomass burning regions due to their higher emissions. Due to the SOA formation, the OM concentrations over Midwest US and Central Siberia are also noticeably high. The sea salt concentrations are distributed fairly uniformly over the oceans but are higher over the Southern Ocean and lower over the oceans near the tropics as expected due to wind speed variations. The dust concentrations are pronounced over the source regions such as Northern Africa, Arabia, Northern/Northwestern China, and Australia.

Figure 7 shows zonal distributions of annual-mean aerosol concentrations in ModelE2-TOMAS. The sulphate concentrations are highest between 0° N and 50° N due to the high anthropogenic emissions in the NH. Over the SH, the sulphate concentrations are mostly a result of DMS oxidation. The zonal-mean EC and OM concentrations are high from the tropics to ~50° N. Similar to Fig. 6, the high EC and OM concentrations are around 30° N to 50° N due to fossil fuel emissions, but the OM concentrations are also large around the tropics due to biomass burning emissions. The two small spikes shown the EC and OM concentrations between 10° S and 10° N are a result of the injection height used in the biomass burning emissions. Since a significant amount of sulfate and OM are also formed through chemical reactions in the atmosphere, their vertical gradients are relatively small. The sea salt concentrations are high from 60° S to 50° N with a peak around 30° S to 60° S due to the large open ocean in the SH. A strong dust plume is shown at around 0°-30° N due to the large Northern African and Middle East dust emissions, and a small dust plume at around 30° S due to Australian emissions. In the model, the PM10 concentrations in upper troposphere are dominated by sulfate and dust particles.

5.3 Aerosol mass concentrations evaluation

The simulated surface-layer mass concentrations of aerosols are evaluated against various observations: 1) sulphate/sea salt/dust concentrations at 23 long-term observation sites operated by University of Miami (e.g. Prospero and Bonatti, 1969; Savoie and Prospero, 1989; Arimoto et al., 1990); 2) speciated PM2.5 concentrations from the Interagency Monitoring of Protected Visual Environment (IMPROVE) sites in the United States that are annual-averages from 2000 to 2008 (Debell et al., 2006; Hand et al., 2011); 3) speciated PM2.5 concentrations from various European observations (Putaud et al., 2010) (hereafter, referred to as European sites); 4) a large set of PM2.5 observations assembled in support of the Global Burden of Disease Study (GBD Study 2010, http://www.globalburden.org); 5) deposition flux measurements obtained from Ginoux et al. (2001), Tegen et al. (2002), and Mahowald et al. (2009). The PM2.5 dataset from the GBD Study consists of a worldwide set of annual-average PM2.5 largely drawn from official monitoring networks for 2005 (in some cases from 2004-2006). The GBD PM2.5 dataset includes the IMPROVE network and the European site measurements, so we only present the PM2.5 evaluation with the GBD dataset. For details of the GBD PM2.5 dataset, the reader is referred to the description in the supplementary material in Shindell et al. (2011).

Figure 8 compares the model annual-mean surface-layer sulphate mass concentrations to the observations from the IMPROVE network, the European sites, and the University of Miami network. Simulated sulphate agrees well with observations, mostly within a factor of two. Compared to ModelE2-OMA, the ModelE2-TOMAS model shows better agreement in the European sites (i.e. LMNB=-0.06 and LMNE=0.13 in Fig. 8b) but worse in the IMPROVE sites (i.e. LMNB=0.06 and LMNE=0.16 in Fig. 8a) and the remote oceanic sites (i.e. LMNB=0.04 and LMNE=0.22 in Fig. 8c). Over the US, both models overpredict systematically at lower observed concentrations (i.e. below 1 $\mu g\ m^{-3}$ of measured SO_4 concentrations), which are mostly located over the western US.

Monthly mean surface-layer sulphate concentrations are evaluated using observations from the University of Miami in Figure 9. The simulated sulphate mass concentrations from both models usually falls within the standard deviation of the observed values. The

sulphate predictions in both ModelE2-OMA and ModelE2-TOMAS become quite similar over the SH because about a factor of two lower DMS emissions are used in ModelE2-TOMAS. Using the same DMS emissions as ModelE2-OMA, ModelE2-TOMAS tends to overpredict sulphate concentrations noticeably over the SH (not shown), and the higher SO_4 concentration with ModelE2-TOMAS could be explained by 1) a longer lifetime due to different deposition parameterizations, 2) letting all SO_4 formed from aqueous oxidation to evaporate without accounting for cloud evaporation, 3) a stronger oxidation state resulted from un-degraded photolysis rates by aerosol optical depth (more SO_4 can be formed from DMS oxidation). Despite the fact that ModelE2-OMA accounts for the heterogeneous SO_4 formation on dust particles, SO_4 concentrations in near dust source regions are still higher in the ModelE2-TOMAS model due to the shorter lifetime in the ModelE2-OMA model.

Simulated annual-mean surface-layer sea salt concentrations are evaluated with the IMPROVE network, the European sites, and the University of Miami network (Fig. 10). Both aerosol models are biased strongly high over the US and Europe but biased low near the tropics. Unlike ModelE2-OMA, ModelE2-TOMAS underpredicts sea salt concentrations at several remote sites (see Fig. 10c). Compared to other aerosol components, the agreement between model sea salt and the observations is worse over the United States and Europe. For the evaluation of monthly mean surface-layer sea salt concentrations against the University of Miami dataset in Figure 11, the model predictions fall within the observed standard deviation at about a half of the 26 sites, but these sites are not necessarily the same between the two aerosol models. The overprediction of sea salt in continents may suggest that ModelE2 has a stronger transport from ocean to in-land, as there is no obvious overprediction over adjacent oceanic sites. The ModelE2-OMA model exhibits a particularly large overprediction over most SH sites. Both models tend to be biased significantly low at some of the sites near the tropics where the observed sea salt concentrations are high. Similar underprediction is also shown in mineral dust (see Fig. 13). This might be due to fast wet scavenging due to overpredicted precipitation in that area (see Fig. 9 in Schmidt et al., 2014).

For ModelE2-TOMAS, simulated annual-mean surface-layer dust concentrations are mostly within a factor of two of the measurements (in Fig. 12): 6 sites are excluded in

Fig. 12 due to an incomplete annual cycle. ModelE2-TOMAS shows good agreement at the IMPROVE and European sites, while ModelE2-OMA tends to underpredict. This is due to the emission size assumptions (resulting in more clay emissions than ModelE2-OMA) and the differences in the deposition parameterizations (resulting in slightly longer lifetime for clay particles; ~9 days in ModelE2-TOMAS and 6.5 days in ModelE2-OMA). Both models are biased low compared to the University of Miami dataset, and only 7-8 sites among 20 sites fall within a factor of two agreement. A few sites show a severe underprediction for both models, mostly located near the tropics and in SH high latitudes.

Monthly mean surface-layer dust concentrations are evaluated using the observations from the University of Miami in Figure 13: no measurement data is available at 3 sites (Reunion Island, Invercargill, and Marion Island), but we still include them to compare the two aerosol model predictions. The model captures the observed annual cycle of dust very well at most NH sites but not in the SH sites except Norfolk and Mawson. The model captures the observed magnitude well at sites located relatively near the source regions (e.g., Sal Island, Barbardos, Bermuda for African dust; Jeju Island and Hedo for Asian dust; Cape Grim and Norfolk Island for Australian dust). Both models underpredict dust concentrations in the NH/SH high latitude (45°) regions except Mace Head, but the simulated dust seems to be within the observed standard deviation as the observations have a large standard deviation for dust. The observed peak concentration at Heimaey Iceland is the second highest after Sal island. Our models underpredict this site severely probably because our dust emission parameterization is not designed to simulate a dust event in humid areas such as Iceland. Prospero et al. (2012) points out that dust emissions at high latitudes (e.g., Alaska and Iceland) are mostly due to individual dust events or single seasons and link large dust events at Heimaey Iceland during 1997 to 2002 with glacial outburst floods.

Figure 14 compares simulated annual-mean dust deposition fluxes against observations obtained from Ginoux et al. (2001), Tegen et al. (2002), and Mahowald et al. (2009). Data is classified by the influencing source region, presented in different colours in Fig. 14. Except for the minor source category, the model dust deposition fluxes tend to be underestimated at most locations and agree with observations only within a

factor of 5-8 on average. This may indicate that dust emissions are too low in ModelE2, but deposition fluxes measurements could contain large particles especially close to source regions (e.g., Duce, 1995) or local emissions (Uematsu et al., 1985) that are not simulated in the model. For ModelE2-TOMAS, the upper size limit being 10 μm, which is too small for the dust particles near the sources, can explain some of the severe underprediction, and Lee et al. (2009) also shows similar disagreement using the GISS-TOMAS model.

Figure 15 shows simulated annual-mean surface-layer EC and OM concentrations compared against the observations from the IMPROVE network and the European sites from Putaud et al. (2010). The simulated EC and OM in both models agree very well at the IMPROVE sites (for EC, LMNB=-0.08 to 0.05; for OM, LMNB=-0.17 to -0.08). Note that we applied an OM/OC ratio of 1.4 to the IMPROVE network to make it consistent with our model assumption, but the IMPROVE OM data provided to us was based on the ratio of 1.8. Over Europe, the model predictions are still reasonable (within a factor of 2-3), but the agreement is slightly worse than the IMPROVE sites. Since these sites are mostly adjacent to the source/emissions, the good agreement suggests that the emission inventory (used in this study) is well represented for these regions.

Figure 16 compares simulated annual-mean PM2.5 concentrations against the GBD dataset. Note that ModelE2-OMA includes nitrate mass into its PM2.5, and the nitrate contributes to PM2.5 rather significantly. The GBD data is classified/presented by a region listed in Figs. 16a and b. The aerosol models capture the observation quite well in most locations (overall LMNB is -0.08 to -0.03 and LMNE is 0.2 to 0.25), but both models show the worst agreement for Oceania regions (LMNB/LMNE=0.4-0.58) and Latin America (LMNB/LMNE =-0.33 to -0.48). The PM2.5 overprediction in Oceania is mainly due to too much fine mode sea-salt particles (the overall agreement in Oceana is little influenced by sulfate or dust particles). Note that the sea salt comparison to the Miami dataset (in Figures 11) shows severe underpredictions in several sites in Oceania because their concentrations are likely dominantly by coarse mode sea salt particles. The underprediction of PM2.5 in Latin America might be related to the biomass burning emissions. It is consistent with the model AOD being biased low over biomass burning source regions that is shown in Section 5.4. Model evaluation with the observed PM10

concentrations using the IMPROVE and European sites was also performed and is similar to the PM2.5 evaluation results (not shown): LMNB and LMNE are -0.01 and 0.17 for ModelE2-TOMAS and 0.0 and 0.29 for ModelE2-OMA, respectively.

5.4 Aerosol optical depth evaluation

Simulated annual-mean clear-sky aerosol optical depths (AODs) at 550 nm are compared with observations from the Terra MODIS (MODerate resolution Image Spectroradiometer; e.g. Abdou et al., 2005; Remer et al., 2008) and MISR (Multiangle Image SpectroRadiometer; e.g. Diner et al., 1998; Kahn et al., 2005) satellite instruments averaged over 2004-2006 (Fig. 17). Specifically, we use Terra MODIS Level 3 (MOD08_M3.051), Aqua MODIS Level 3 (MYD08_M3.051), and Terra MISR Level 3 (MIL3MAE4), which are monthly products with 1x1 degree resolution. We also use the Deep Blue AOD (e.g., Hsu et al., 2006) from Terra MODIS to increase its spatial coverage, and all the satellite data was obtained from http://disc.sci.gsfc.nasa.gov/giovanni. When the Deep Blue AOD and the "regular" AOD from Terra MODIS are both available, the former is used. However, we notice that the Deep Blue AOD shows some local hotspots (e.g. over South America) that are not shown in the "regular" MODIS AOD as well as the MISR AOD. Our model calculates clear-sky AOD by including only AOD values calculated in model locations where clouds are not present (i.e., cloud-free grid-box only). The ModelE2-TOMAS and ModelE2-OMA models capture the broad spatial features seen in the satellite measurements: 1) very high AODs over desert regions in and near Northern Africa and the Arabian Peninsula associated with mineral dust, 2) the band of locally enhanced AOD over the Southern Ocean associated with sea salt, 3) high AODs over East Asia and India due to high anthropogenic emissions. However, the models underestimate the AOD over East Asia and the Indo-Gangetic plain, especially compared to MODIS. Including nitrate in ModelE2-OMA, the AOD predictions increase particularly over Europe and East Asia. Without nitrate, they become quite similar to the ModelE2-TOMAS AOD values in the regions where the model nitrate predictions are significant. The models show an enhanced AOD over the biomass burning regions such as tropical South America, Africa and Indonesia but it is clearly underestimated. The simulated AOD in North America and

high latitude regions appears also to be lower than the satellite observations. Comparing with ModelE2-OMA AOD, ModelE2-TOMAS shows a stronger AOD over Africa due to its higher dust burden and a lower AOD over the marine areas especially the Southern Ocean associated with sea salt.

We present spatial correlations and biases between the models and the satellite data (Table 6). For these analyses, the annual-mean satellite AOD fields are regridded to 2°x2.5° horizontal resolution, and the models are sampled only where the satellite AOD is available. Correlation coefficients between the model and satellite AODs are around 0.6-0.7 for ModelE2-TOMAS and around 0.4-0.5 for ModelE2-OMA. Given that the correlation coefficient between MODIS and MISR is 0.79, the ModelE2-TOMAS model shows a good correlation with these satellite data. Both models show better correlations with MISR AOD. Compared to ModelE2-OMA, ModelE2-TOMAS shows a strong negative bias (about -29 to -34%) for both satellite datasets because of noticeably low AODs over the oceanic regions (where sea salt is dominant) shown in Fig. 16 and possibly because of missing component such as nitrate aerosols, which contributes to AOD significantly over Europe and China in the ModelE2-OMA model. Over Europe, the ModelE2-OMA model overpredicts AOD due to nitrate though. Without nitrate in ModelE2-OMA, the normalized mean bias (NMB) falls from 8-16% to -16 to -21%. Both models show lower AOD over China, India, and biomass burning regions and a similar underprediction is shown in by the ACCMIP models (Shindell et al., 2013), indicating a possibility of aerosol emissions being underestimated in these regions.

Figure 18 presents simulated monthly mean AODs compared against AERONET (AErosol RObotic NETwork; Holben et al., 1998; Holben et al., 2001) measurements at 28 sites that represent the following characteristic regions: polluted continental, marine, biomass-burning, and dusty regions (see Table 7 for individual site information). Both ModelE2-TOMAS and ModelE2-OMAunderestimate the maximum AOD during summer by a factor of 2-3 in the biomass burning sites (1 to 6) but capture the observed annual cycle quite well (R>~0.9). Unlike other biomass burning sites, simulated AODs at Ilorin and Banizoumbou are comparable to the observations possibly due to the influence of mineral dust. The agreement between the models and the AERONET AOD is generally good in the dusty regions (9 to 16). The ModelE2-TOMAS model shows a

slight overprediction of AOD during spring at Capo Verde and Bidi Bahn which are located near the African dust sources, although it shows a good agreement at Barbados where is also influenced by African dust.

For ModelE2-TOMAS, all polluted continental sites (17 to 24) show large underpredictions, while the model tends to capture the observed annual cycle well. However, the model surface aerosol mass concentrations agree well with the observations from IMPROVE network and several European sites (see Figs. 8, 10, 12, 15, and 16). This might be due to the fact that column AOD depends on many additional factors (e.g., optical properties and vertical distribution of aerosols) and provides a measure of total radiatively active aerosols in the atmosphere. Misrepresentation of these factors or missing a chemical component could introduce a bias in the model AODs. For ModelE2-OMA, the model AOD without nitrate is quite similar to the ModelE2-TOMAS AOD. Including nitrate in ModelE2-OMA, it simulates the annual-mean AERONET AOD relatively well but the observed annual cycle worse. Although the inclusion of nitrate is helpful for the underpredicted AOD in polluted regions, the overprediction of wintertime AOD suggests that the model nitrate is too large.

With the ModelE2-TOMAS model, the oceanic sites (25 to 30) are generally underpredicted roughly by a factor of two except for Bermuda (25) and Lanai (26). By contrast, the ModelE2-OMA model captures the observed magnitude relatively well but overpredicts at Bermuda and Lanai. Note that Bermuda (23) and Rottnest Island (27) are influenced by long-range transported mineral dust. The ModelE2-OMA model predicts AOD that is more comparable to observations in these oceanic sites than ModelE2-TOMAS. Compared to ModelE2-OMA, the underprediction of sea salt concentrations at the remote sites (shown in Figs. 10 and 11 in Sect. 5.3) and the underpredictions of AODs in the remote oceanic sites in ModelE2-TOMAS may be due to a faster sea salt removal rate (see global budgets in Table 4 for the details). It is worth mentioning that the inclusion of marine organic aerosols, which are not included in this paper, may not increase AOD noticeably in remote oceanic sites. Using the same host model, Tsigaridis et al. (2013) shows that Southern Ocean AOD is quite insensitive to the inclusion of marine organic particles but is strongly sensitive to the sea-salt emissions parameterization (see Figure 9 of Tsigaridis et al. (2013).

5.5 Aerosol number budgets and its distributions

This section includes only ModelE2-TOMAS results, as ModelE2-OMA does not predict aerosol number concentrations. Global mean number budgets for all three simulations, including two sensitivity runs for nucleation rates, are presented in Table 8 (see Section 4.2 and Table 1 for the details of run descriptions). Compared to the BASE run, global mean CN3 (particles with dry diameters larger than 3 nm), CN10 (particles with dry diameters larger than 10 nm), and CN100 (particles with dry diameters larger than 100 nm) concentrations in the LowNUC run are decreased by 74%, 33%, and 7% in the troposphere and 29%, 17%, and 3% in the lowermost layer, respectively. The smaller impact on CN in the lowermost layer is due to the presence of the primary emissions near the surface. It is also because the binary nucleation parameterization used in this model produces few particles in the boundary layer; however, nucleated particles in the upper/free troposphere may be carried down to the surface and influence CN there. Since the LowNUC run produces fewer nucleated particles than the BASE run, each nucleated particle is more likely to grow more efficiently to form CCN-sized particles, as there is less competition for sulphuric acid and condensable organics. We can see this using the number budgets in Table 8. The increase in CN70 with the BASE case nucleation (i.e., BASE CN70 – NONUC CN70) is 51 cm^{-3} for the nucleation rate (J3) of 0.131 cm^{-3} s^{-1} and that with the LowNUC case nucleation, 37 cm^{-3} for J3 of 0.013 cm^{-3} s^{-1}. In the BASE run, J3 is 10 times higher but the CN70 increase by nucleation is only ~1.4 times higher than those in the LowNUC run.

Aerosol number burdens normalized by tropospheric volume are dramatically reduced when nucleation is turned off in the NoNUC run. For example, global mean CN3 and CN10 are decreased by 95% and 76% in the troposphere and by 42% and 31% in the surface layer. We found that 24% of tropospheric CCN-sized particles (i.e., CN100) and ~10% of surface-layer CCN-sized particles result from binary nucleation in our model; the contribution of the nucleated particles to the CCN concentrations is larger as the cutoff size (e.g. 100 nm in CN100) gets lower.

Figure 19 shows global distributions of annually averaged CN3, CN10, and CN100 in the lowermost layer for the BASE, LowNUC, and NoNUC runs, and Fig. 20 presents their zonal distributions. For the CN3 distributions, the BASE run shows a high

concentration (over 5000 cm^{-3}) in the upper/free troposphere and the entire Antarctica troposphere due to nucleation and over polluted continental regions due to the primary emissions (see Figs. 19a and 20a). Note that the CN3 near the surface in Antarctica comes from nucleated particles from the upper/free troposphere, as the binary parameterization does not predict nucleation in the boundary layer. CN3 in the LowNUC run (Figs. 19d and 20d) is decreased significantly in the free troposphere and in the surface layer over Eurasia and western Antarctica (fewer nucleated particles formed above subside to the surface). When nucleation is switched off, CN3 is very close to CN10 near to the surface (Figs. 19g and h) because nucleation contributes most CN between 3 nm to 10nm. For CN10, its spatial pattern over the continents is quite similar among the runs as it is mostly driven by primary emissions except for some locations heavily influenced by the nucleated particles formed in the upper/free troposphere (Figs. 19b, e and h and Figs. 20b, e, h). A pronounced difference in CN10 is shown over oceans, indicating a larger contribution of nucleated particles to CN10 in these regions. This is consistent with Merikanto et al. (2009), which shows higher contribution of nucleation to CN over oceanic regions. CN100 differs little among runs except for SH high latitudes where binary nucleation plays an important role (Figs. 19c, f, and i). This is consistent with Pierce and Adams (2009) showing that the exhibited high SH latitude region for the most positive changes in CCN(0.2%) by turning on binary nucleation and, again, with Merikanto et al. (2009) showing 65% of CCN(0.2%) in Antarctica resulted from upper tropospheric nucleation. CN100 shows a maximum at 10° N to 40° N because most anthropogenic primary emissions are located in mid-NH latitudes. Rather surprisingly, dust particles in our model contribute to CN100 quite significantly over the source regions. This is opposite to the results from GISS-TOMAS (Lee et al., 2009), which shows a 10-20% reduction in CCN(0.2%) when introducing mineral dust emissions. Despite the direct source of CCN-sized particles from dust emissions, CCN and ultrafine particles that grow to become CCN are scavenged via coagulation with coarse dust particles, and dust particles compete for condensable sulfuric acid, leading to a slower growth rate of ultrafine particles.

5.6 Aerosol number evaluation

The CN measurement dataset compiled by Spracklen et al. (2010) is used to evaluate simulated annual-mean CN concentrations (in Fig. 21) and monthly mean CN concentrations (in Fig. 22). Details of the measurement procedures for each site, including the instrument type and minimum cutoff diameter (varying from 3nm to 14 nm), can be found in Table 2 of Spracklen et al. (2010). Due to an incomplete annual cycle, we excluded Mt. Waliguan, Finokalia, Listvyanka, and Weybourne. The measurement sites are classified into three categories: FT (free troposphere; 1 to 8 in Fig. 22), MBL (marine boundary layer; 9 to 15 in in Fig. 22), and CBL (continental boundary layer; 16 to 32 in Fig. 22). We sampled the model values to match the altitude of each measurement site except for the free troposphere sites that use an altitude 30% lower because it improved the annual cycles prediction significantly. Previous studies pointed out that free tropospheric sites can be influenced by upslope winds that carry the planetary boundary layer air, so it cannot be assumed to be in the free troposphere all the time (e.g., Baltensperger, 1997; Collaud Coen et al., 2011). Our model does not seem to simulate this well, so sampling the model predictions at lower altitude (i.e., 30% lower) helps to increase the influence of PBL air. In Fig. 21, a whisker plot is used to present the three run results; the maximum of the whisker line for the BASE run; the circle symbol in the middle of the whisker line for the LowNUC run; the minimum for the NoNUC run.

On average, the annual-mean CN concentrations in the model agree with the observations well for the all three categories (LMNB= -0.26 to 0.16; LMNE=0.13 to 0.22; see Fig. 21), although the LowNUC simulation shows the best agreement to observation. Simulated annual cycles at individual sites also show that the model captures the measured magnitude reasonably but overpredicts the CN during winter (November to March) that is worse at the CBL sites and results in poor seasonality (especially in the BASE run). The poor seasonality in ModelE2-TOMAS in all three runs suggests that other factors may play a role such as missing seasonal variation in primary emissions or scavenging that causes the poor seasonality rather than nucleation. The evaluation of CN at South Pole shows that the model predicts too strong nucleation throughout the year.

Figure 23 compares the observed size distributions at six European sites during winter (DJF: December to February; Figs. 23a to f) and summer (JJA: June to August; Figs. 23d to l) to the model. The observed size distributions are averaged during morning,

afternoon, and night, while the model results are not broken into the three periods. This data is obtained from Putaud et al. (2003) and, for the same sites shown in Figure 21, the temporal coverage used in Putaud et al. (2003) is not necessarily matched with them. Most sites are reasonably close to the dataset used in Figure 21. However, for Jungfraujoch, the total CN concentrations summed from the size distribution data, which covers from June 1997 to May 1998, is about a factor of two lower than the CN shown in Figure 21, which covers from 1995 to 1999 and 2003-2007. As expected, the simulated size distributions of the model simulations differ according to what nucleation scheme is used. The impact of nucleation is more notable for particles smaller than ~50 nm, as expected, and also during winter. In general, the higher nucleation rates tend to overpredict Aitken model particles at most sites. For Harwell (Figs. 23c and i), particles below 50 nm are overpredicted even without nucleation. For the summer season, the model shows less sensitivity to nucleation rates and has better skill at capturing the observed size distributions.

The observed CN5, CN15, and CN120 concentrations from the LACE campaign (Petzold et al., 2002) are compared with three model runs (Figs. 24a to c). Below 700-800 mbar, all three model runs predict concentrations roughly within the observed CN5, CN15, and CN120 ranges. Above 700-800 mbar, the BASE simulation overpredicts CN5 and CN15 by approximately an order of magnitude and 2-3 times, respectively. For the NoNUC simulation, it captures the lower side of the observed CN15 but fails to capture the increasing CN5 concentrations with height above 600 mbar. All model runs basically show almost identical CN120 concentrations and fall on the lower edge of the observed range.

We compare CN3 vertical profile measurements averaged into the 3 latitude bands over the Pacific Ocean (Clarke and Kapustin, 2002) with the model (Figs. 24 d to f). The simulated CN3 profiles in LowNUC agree well with the observation, capturing the increasing CN3 with height. Although the BASE run shows the increasing pattern correctly, it overpredicts CN3 severely above approximately 6 km. The NoNUC run disagrees with the observations for all latitudes and altitutes and clearly fails to reproduce the high number concentrations in the upper troposphere that result from nucleation.

The observed Aitken mode and accumulation mode concentrations and size distributions in the marine boundary layer (Heintzenberg et al., 2000) are compared with the model in Figs. 25 and 26. The measurements are aggregated into 15-degree latitude ranges. For the Aitken mode (Fig. 25a), the LowNUC run shows the closest agreement to observations. However, whereas the observations show higher concentrations in the SH than in the NH, all model simulations show the opposite tendency. Similarly, other global models with binary nucleation show underpredicted CN concentrations in the SH and either well-simulated or overpredicted CN in the NH (e.g. Easter et al., 2004; Spracklen et al., 2005; Pierce and Adams, 2006; Pierce et al., 2007; Trivitayanurak et al., 2008; Mann et al., 2010; Wang et al., 2011). For the accumulation mode (Fig. 25b), the three model runs are quite similar to each other and are within the observed range.

In Fig. 26, ModelE2-TOMAS captures the bimodal size distribution shown in the observations reasonably, which is mainly determined by the activation diameter assumed in wet deposition (and cloud processing): ~80 nm as an activation diameter (supersaturation of 0.2%) for both large-scale clouds and convective clouds in the model. Note that ModelE2-TOMAS cannot capture the observed bimodal distribution when a supersaturation of 1.0% is assumed for convective clouds, unlike the other TOMAS models (e.g. Pierce et al., 2007;Trivitayanurak et al., 2008): a peak at around 20-30 nm appears when the supersaturation of 1.0% is assumed for convective clouds. This suggests that, compared to GISS GCM II', convective clouds are more frequent in ModelE2. Although the model captures the observations successfully using fixed supersaturation assumptions, future work is needed to link the in-cloud supersaturation to cloud and aerosol properties.

Simulated CCN concentrations are compared against a dataset of CCN measurements compiled by Spracklen et al. (2011) in Figs. 27 and 28: see Table 1 in Spracklen et al. (2011) for the details regarding each site. The CCN dataset includes a total of 277 measurements at 80 locations using various instruments from 1971 to 2009. Approximately 70% of the observations were taken after 1990. Most have sampling periods of days to weeks except the observations at Cape Grim and Mace Head. For Cape Grim and Mace Head, an annual cycle is available, so we present them separately in Fig. 28. In Fig. 27, the CCN data is divided into two groups: CCN in the MBL (marine

boundary layer) and CCN in the CBL (continental boundary layer). Note that all CCN measurements used here are in the boundary layer. For CCN in the CBL, the model CCN shows good agreement with the observation in all three simulations (LMNB=0.11-0.2 and LMNE=0.31-0.34). For CCN in the MBL, the model predictions are, on average, within a factor of 1.5-2 of the observations for all three runs but, relative to several measurements of CCN concentration between ~100 and ~300 cm^{-3}, are biased high, by roughly a factor of two.

For the annual cycle of CCN concentrations at Cape Grim and Mace Head (Fig. 28), the model overpredicts in all months even without nucleation (NMB>1.0). The CCN overpredictions at Cape Grim might be influenced by overpredicted SO_2 (shown in Fig. 3), which could lead to overpredicted condensational growth of Aitken mode particles. As with the SO_2 evaluation in Fig. 3, the CCN overprediction decreases by sampling adjacent grids toward the ocean (not shown), but the model CCN is still higher than the measurements. Given the fact that most CCN observations have very short duration (days to weeks) in a single year and, according to Spracklen et al. (2011), the relative uncertainties in the measurement data range from about 5-40%, mostly in 10-20% very roughly, the overall model-to-observation agreement is satisfactory.

6. Conclusions

We have implemented the TwO-Moment Aerosol Sectional (TOMAS) microphysics model into the new version of the GISS GCM (i.e. ModelE2), called "ModelE2-TOMAS". This paper has compared the global budgets of ModelE2-TOMAS to other global aerosol models and evaluates the model with various observations such as aerosol precursor gas concentrations, aerosol mass and number concentrations, and aerosol optical depth.

Global budgets of aerosols and aerosol precursor gases in ModelE2-TOMAS are similar to those in other global aerosol models, and the ModelE2-TOMAS model agrees reasonably (mostly within a factor of two) with long-term observed aerosol precursor gas and aerosol mass concentrations. The model captures the broad spatial features shown in the MODIS and MISR annual-mean AOD distributions as well as the observed seasonal

trends of AOD at several AERONET sites. The model predicts the observed annual-mean CN (the minimum cutoff varying from 3nm to 14 nm) concentrations very well and the observed vertical profiles of aerosol number over Germany (i.e., LACE campaign) and in the marine boundary layer. For CCN, the model shows good skill in capturing the observations. We conclude that the model is realistic enough to be useful for many types of scientific study.

However, the evaluation has also highlighted some weaknesses in ModelE2-TOMAS to be revisited in the future. First, ModelE2-TOMAS predicts too much SO_2 lifted into the upper/free troposphere over the Pacific Ocean possibly due to overly strong convective transport. This is also seen in ModelE2-OMA (and in gaseous tracers), suggesting this might be a host model problem. Second, the model AOD is underpredicted over polluted continents, even though mass concentrations of each aerosol component at the surface are well simulated (or at least not underpredicted) in the model. Missing nitrate in ModelE2-TOMAS may not be the main contributor, as the inclusion of nitrate in ModelE2-OMA decreases its ability to capture the observed seasonality in AERONET polluted continents sites. Third, the model tends to underpredict aerosol loading (and AOD) over biomass burning emission regions. This is a common issue in global aerosol models, and this might be due to underestimation of biomass burning emissions. Fourth, the ModelE2-TOMAS AOD prediction is biased low over the SH high-latitude oceans, which suggests underpredicted sea salt burden in this area. Fifth, the simulated CN seasonality is poor at some CBL sites due to overpredicted CN during the wintertime. Similarly, ModelE2-TOMAS predicts the observed number size distributions over European sites during the summer season reasonably but not for the winter season. The model overpredicts Aitken mode particles during the winter season, which happens even without nucleation, possibly due to a problem in primary emissions representation or a bias in the model scavenging that causes the poor seasonality. Finally, ModelE2-TOMAS seems to predict faster nucleation rates using binary nucleation (Vehkamaki et al., 2002) than other global microphysics models using the same binary nucleation (including GISS-TOMAS). For instance, the observed CN vertical profiles are captured the best when nucleation rates are reduced (our LowNUC run), while Lauer et al. (2005) presents significantly underpredicted CN profiles with the same binary nucleation scheme

using ECHAM/MADE. To investigate this issue further, we need to perform a model evaluation against observation-derived nucleation-relevant metrics, which has been done in Westervelt et al. (2013). Because of the fine size assumptions for the primary emissions (see Section 4.2 for the details) and/or the fast nucleation rates using binary nucleation in ModelE2-TOMAS, we do not include boundary nucleation as it overpredicted CN near the surface. We conclude that further work is necessary to improve the realism of some aspects of ModelE2-TOMAS and to better understand the size-resolved physical processes (e.g. microphysics, emissions, and depositions).

Comparing the ModelE2-TOMAS model with the ModelE2-OMA model in ModelE2, some aerosol species burdens and concentrations differ significantly, even with using the same host model and identical anthropogenic emissions, mainly because the deposition parameterizations and some of the emission-related assumptions are different. In the case of sea salt and dust, the size ranges assumed by each model are different, resulting in different emission rates and burdens.

Analysis of multiple aerosol model results help to identify where a model bias might originate from: aerosol modelling or the host GCM or elsewhere such as emissions. We found that some of the large differences in aerosol predictions between the two aerosol models are due to aerosol modelling. This is valuable information, as this is not easy to constrain using observations. Having more than one aerosol physics representation in the NASA GISS ModelE2 will serve as a useful tool to study the uncertainty in aerosol modelling and to guide our efforts to improve the models.

Code Availability

Currently, we do not have a publicly available version of either NASA GISS ModelE2-TOMAS or ModelE2 itself. The ModelE2-TOMAS code may be provided upon the request. However, it may be quite challenging to compile and run ModelE2-TOMAS in a new computer environment as the model has been developed in a NASA NCCS supercomputer (http://www.nccs.nasa.gov/discover_front.html) and a user manual has not been developed.

It is worth noting that the public version of ModelE2 (the TOMAS model is not a part of standard version of ModelE2) will be available in the next few years, and the NASA GISS ModelE (which has been used for IPCC AR4 simulations) is publicly available: see details in http://www.giss.nasa.gov/tools/modelE/.

Acknowledgements

Funding for this research was supported by NASA ACMAP and MAP program. Resources supporting the simulations were provided by the NASA High-End Computing (HEC) Program through the NASA Center for Climate Simulation (NCCS) at Goddard Space Flight Center. We gratefully acknowledge the mission scientists and Principal Investigators who provided the data used in this research effort (EMEP, CASTNET, IMPROVE, and University of Miami networks, AERONET, NASA MODIS and MISR). We also acknowledge the PIs for the CN and CCN surface measurements at the WMO-GAW sites (J. Ogren, Earth System Research Laboratory, NOAA, US; J. Gras, CSIRO Marine and Atmospheric Research, Australia; U. Baltensperger, Paul Scherrer Institute, Switzerland; U. Kaminski, Deutscher Wetterdienst (DWD), Germany; S.G. Jennings, National University of Ireland Galway, Ireland; R. Weller, Alfred Wegener Institute for Polar and Marine Research, Germany; Y. Viisanen, Finnish Meteorological Institute, Finland). We further acknowledge that Cape Grim data are provided by the Australian Bureau of Meteorology (Cape Grim Baseline Air Pollution Station) and CSIRO Ocean and Atmosphere Flagship. We thank Graham Mann (University of Leeds, UK) and Dominick Spracklen (University of Leeds, UK) for providing aerosol number measurements data collection. We also thank Greg Faluvegi (NASA GISS) and Maxwell Kelley (NASA GISS) for providing technical support during the model development. Finally, we thank two anonymous reviewers for constructive comments and suggestions that have improved the paper considerably.

References

Abdou, W. A., Diner, D. J., Martonchik, J. V., Bruegge, C. J., Kahn, R. A., Gaitley, B. J., Crean, K. A., Remer, L. A., and Holben, B.: Comparison of coincident Multiangle Imaging Spectroradiometer and Moderate Resolution Imaging Spectroradiometer aerosol optical depths over land and ocean scenes containing Aerosol Robotic Network sites, J. Geophys. Res.-Atmos., 110, D10S07, doi: 10.1029/2004jd004693, 2005.

Adams, P. J., and Seinfeld, J. H.: Predicting global aerosol size distributions in general circulation models, J. Geophys. Res.-Atmos., 107, 4370, doi:10.1029/2001JD001010, 2002.

Andres, R. J., and Kasgnoc, A. D.: A time-averaged inventory of subaerial volcanic sulfur emissions, Journal of Geophysical Research: Atmospheres, 103, 25251-25261, 10.1029/98JD02091, 1998.

Arimoto, R., Ray, B. J., Duce, R. A., Hewitt, A. D., Boldi, R., and Hudson, A.: CONCENTRATIONS, SOURCES, AND FLUXES OF TRACE-ELEMENTS IN THE REMOTE MARINE ATMOSPHERE OF NEW-ZEALAND, J. Geophys. Res.-Atmos., 95, 22389-22405, 10.1029/JD095iD13p22389, 1990.

Ayers, G. P., Ivey, J. P., and Gillett, R. W.: COHERENCE BETWEEN SEASONAL CYCLES OF DIMETHYL SULFIDE, METHANESULFONATE AND SULFATE IN MARINE AIR, Nature, 349, 404-406, 10.1038/349404a0, 1991.

Baltensperger, U.: Aerosol climatology at the high,ÄêAlpine site Jungffaujoch, Switzerland, Journal of Geophysical Research, 102, 19707-19715, 1997.
Bauer, S. E., and Koch, D.: Impact of heterogeneous sulfate formation at mineral dust surfaces on aerosol loads and radiative forcing in the Goddard Institute for Space Studies general circulation model, J. Geophys. Res.-Atmos., 110, D17, D17202, doi: 10.1029/2005jd005870, 2005.
Bauer, S. E., Koch, D., Unger, N., Metzger, S. M., Shindell, D. T., and Streets, D. G.: Nitrate aerosols today and in 2030: a global simulation including aerosols and tropospheric ozone, Atmospheric Chemistry and Physics, 7, 5043-5059, 2007.
Bauer, S. E., Wright, D. L., Koch, D., Lewis, E. R., McGraw, R., Chang, L. S., Schwartz, S. E., and Ruedy, R.: MATRIX (Multiconfiguration Aerosol TRacker of mIXing state): an aerosol microphysical module for global atmospheric models, Atmospheric Chemistry and Physics, 8, 6003-6035, 2008.
Bian, H. S., and Prather, M. J.: Fast-J2: Accurate simulation of stratospheric photolysis in global chemical models, Journal of Atmospheric Chemistry, 41, 281-296, 10.1023/a:1014980619462, 2002.
Boucher, O., Moulin, C., Belviso, S., Aumont, O., Bopp, L., Cosme, E., von Kuhlmann, R., Lawrence, M. G., Pham, M., Reddy, M. S., Sciare, J., and Venkataraman, C.: DMS atmospheric concentrations and sulphate aerosol indirect radiative forcing: a sensitivity study to the DMS source representation and oxidation, Atmos. Chem. Phys., 3, 49-65, 10.5194/acp-3-49-2003, 2003.
Boucher, O., Randall, D., Artaxo, P., Bretherton, C., Feingold, G., Forster, P., Kerminen, V.-M., Kondo, Y., Liao, H., Lohmann, U., Rasch, P., Satheesh, S. K., Sherwood, S., Stevens, B., and Zhang, X. Y.: Clouds and Aerosols. In: Climate Change 2013: The Physical Science Basis. , Contribution of Working Group I to the Fifth Assessment Report of the Intergovernmental Panel on Climate Change, Cambridge University Press. Cambridge, United Kingdom and New York, NY, USA, 571-657, 2013.
Bowman, K. W., Shindell, D. T., Worden, H. M., Lamarque, J. F., Young, P. J., Stevenson, D. S., Qu, Z., de la Torre, M., Bergmann, D., Cameron-Smith, P. J., Collins, W. J., Doherty, R., Dalsoren, S. B., Faluvegi, G., Folberth, G., Horowitz, L. W., Josse, B. M., Lee, Y. H., MacKenzie, I. A., Myhre, G., Nagashima, T., Naik, V., Plummer, D. A., Rumbold, S. T., Skeie, R. B., Strode, S. A., Sudo, K., Szopa, S., Voulgarakis, A., Zeng, G., Kulawik, S. S., Aghedo, A. M., and Worden, J. R.: Evaluation of ACCMIP outgoing longwave radiation from tropospheric ozone using TES satellite observations, Atmospheric Chemistry and Physics, 13, 4057-4072, 10.5194/acp-13-4057-2013, 2013.
Cakmur, R. V., Miller, R. L., Perlwitz, J., Geogdzhayev, I. V., Ginoux, P., Koch, D., Kohfeld, K. E., Tegen, I., and Zender, C. S.: Constraining the magnitude of the global dust cycle by minimizing the difference between a model and observations, J. Geophys. Res.-Atmos., 111, D06207, doi:10.1029/2005jd005791, 2006.
Clarke, A. D., and Kapustin, V. N.: A pacific aerosol survey. Part I: A decade of data on particle production, transport, evolution, and mixing in the troposphere, Journal of the Atmospheric Sciences, 59, 363-382, 10.1175/1520-0469(2002)059<0363:apaspi>2.0.co;2, 2002.
Collaud Coen, M., Weingartner, E., Furger, M., Nyeki, S., Prévôt, A. S. H., Steinbacher, M., and Baltensperger, U.: Aerosol climatology and planetary boundary influence at the

Jungfraujoch analyzed by synoptic weather types, Atmos. Chem. Phys., 11, 5931-5944, 10.5194/acp-11-5931-2011, 2011.
Debell, L. J., Gebhart, K. A., Malm, W. C., Pitchford, M. L., Schichtel, B. A., and White, W. H.: Spatial and seasonal patterns and temporal variability of haze and its constituents in the United States: report IV, 2006.
Del Genio, A. D., Yao, M. S., Kovari, W., and Lo, K. K. W.: A prognostic cloud water parameterization for global climate models, J Climate, 9, 270-304, 1996.
Del Genio, A. D., and Yao, M-S: Efficient cumulus parameterization for long-term climate studies: The GISS scheme, The Representation of Cumulus Convection in Numerical Models, American Meteorological Society, Boston, Mass., 181- 184 pp., 1993.
Dentener, F., Kinne, S., Bond, T., Boucher, O., Cofala, J., Generoso, S., Ginoux, P., Gong, S., Hoelzemann, J. J., Ito, A., Marelli, L., Penner, J. E., Putaud, J. P., Textor, C., Schulz, M., van der Werf, G. R., and Wilson, J.: Emissions of primary aerosol and precursor gases in the years 2000 and 1750 prescribed data-sets for AeroCom, Atmospheric Chemistry and Physics, 6, 4321-4344, 2006.
Dick, W. D., Saxena, P., and McMurry, P. H.: Estimation of water uptake by organic compounds in submicron aerosols measured during the Southeastern Aerosol and Visibility Study, J. Geophys. Res.-Atmos., 105, 1471-1479, 10.1029/1999jd901001, 2000.
Diner, D. J., Beckert, J. C., Reilly, T. H., Bruegge, C. J., Conel, J. E., Kahn, R. A., Martonchik, J. V., Ackerman, T. P., Davies, R., Gerstl, S. A. W., Gordon, H. R., Muller, J. P., Myneni, R. B., Sellers, P. J., Pinty, B., and Verstraete, M. M.: Multi-angle Imaging SpectroRadiometer (MISR) - Instrument description and experiment overview, Ieee Transactions on Geoscience and Remote Sensing, 36, 1072-1087, 10.1109/36.700992, 1998.
Duce, R. A.: Sources, distributions, and fluxes of mineral aerosols and their relationship to climate, Aerosol Forcing of Climate, edited by: Charlson, R. J., and Heintzenberg, J., 43-72 pp., 1995.
Easter, R. C., Ghan, S. J., Zhang, Y., Saylor, R. D., Chapman, E. G., Laulainen, N. S., Abdul-Razzak, H., Leung, L. R., Bian, X. D., and Zaveri, R. A.: MIRAGE: Model description and evaluation of aerosols and trace gases, J. Geophys. Res.-Atmos., 109, D20210, doi:10.1029/2004JD004571, 2004.
Emmons, L. K., Hauglustaine, D. A., Muller, J. F., Carroll, M. A., Brasseur, G. P., Brunner, D., Staehelin, J., Thouret, V., and Marenco, A.: Data composites of airborne observations of tropospheric ozone and its precursors, J. Geophys. Res.-Atmos., 105, 20497-20538, 10.1029/2000jd900232, 2000.
Feingold, G., Tzivion, S., and Levin, Z.: EVOLUTION OF RAINDROP SPECTRA .1. SOLUTION TO THE STOCHASTIC COLLECTION BREAKUP EQUATION USING THE METHOD OF MOMENTS, Journal of the Atmospheric Sciences, 45, 3387-3399, 10.1175/1520-0469(1988)045<3387:eorspi>2.0.co;2, 1988.
Forster, P., and Ramaswamy, V.: Changes in Atmospheric Constituents and in Radiative Forcing, Climate Change 2007: The Physical Science Basis, edited by: Solomon, S., Qin, D., Manning, M., Marquis, M., Averyt, K., Tignor, M. M. B., Miller, H. L., and Chen, Z. L., 129-234 pp., 2007.

Ginoux, P., Chin, M., Tegen, I., Prospero, J. M., Holben, B., Dubovik, O., and Lin, S. J.: Sources and distributions of dust aerosols simulated with the GOCART model, J. Geophys. Res.-Atmos., 106, 20255-20273, 2001.
Gong, S. L.: A parameterization of sea-salt aerosol source function for sub- and super-micron particles, Global Biogeochemical Cycles, 17, 1097, doi:10.1029/2003gb002079, 2003.
Hand, J. L., Copeland, S. A., Day, D. E., Dillner, A. M., Indresand, H., Malm, W. C., McDade, C. E., Moore, C. T., Pitchford, M. L., Schichtel, B. A., and Watson, J. G.: Spatial and Seasonal Patterns and Temporal Variability of Haze and its Constituents in the United States: Report V, Colo. State Univ., Fort Collins, 2011.
Hansen, J., Russell, G., Rind, D., Stone, P., Lacis, A., Lebedeff, S., Ruedy, R., and Travis, L.: Efficient 3-Dimensional Global-Models for Climate Studies - Model-I and Model-Ii, Mon Weather Rev, 111, 609-662, 1983.
Harrington, D. Y., and Kreidenweis, S. M.: Simulations of sulfate aerosol dynamics - Part II. Model intercomparison, Atmospheric Environment, 32, 1701-1709, 10.1016/S1352-2310(97)00453-6, 1998.
Heintzenberg, J., Covert, D. C., and Van Dingenen, R.: Size distribution and chemical composition of marine aerosols: a compilation and review, Tellus Series B-Chemical and Physical Meteorology, 52, 1104-1122, 10.1034/j.1600-0889.2000.00136.x, 2000.
Hoell, J. M., Davis, D. D., Jacob, D. J., Rodgers, M. O., Newell, R. E., Fuelberg, H. E., McNeal, R. J., Raper, J. L., and Bendura, R. J.: Pacific Exploratory Mission in the tropical Pacific: PEM-Tropics A, August-September 1996, J. Geophys. Res.-Atmos., 104, 5567-5583, 10.1029/1998jd100074, 1999.
Holben, B. N., Eck, T. F., Slutsker, I., Tanre, D., Buis, J. P., Setzer, A., Vermote, E., Reagan, J. A., Kaufman, Y. J., Nakajima, T., Lavenu, F., Jankowiak, I., and Smirnov, A.: AERONET - A federated instrument network and data archive for aerosol characterization, Remote Sensing of Environment, 66, 1-16, 10.1016/s0034-4257(98)00031-5, 1998.
Holben, B. N., Tanre, D., Smirnov, A., Eck, T. F., Slutsker, I., Abuhassan, N., Newcomb, W. W., Schafer, J. S., Chatenet, B., Lavenu, F., Kaufman, Y. J., Castle, J. V., Setzer, A., Markham, B., Clark, D., Frouin, R., Halthore, R., Karneli, A., O'Neill, N. T., Pietras, C., Pinker, R. T., Voss, K., and Zibordi, G.: An emerging ground-based aerosol climatology: Aerosol optical depth from AERONET, J. Geophys. Res.-Atmos., 106, 12067-12097, 10.1029/2001jd900014, 2001.
Hsu, N. C., Tsay, S. C., King, M. D., and Herman, J. R.: Deep blue retrievals of Asian aerosol properties during ACE-Asia, Ieee Transactions on Geoscience and Remote Sensing, 44, 3180-3195, 10.1109/tgrs.2006.879540, 2006.
Jourdain, B., and Legrand, M.: Seasonal variations of atmospheric dimethylsulfide, dimethylsulfoxide, sulfur dioxide, methanesulfonate, and non-sea-salt sulfate aerosols at Dumont d'Urville (coastal Antarctica) (December 1998 to July 1999), J. Geophys. Res.-Atmos., 106, 14391-14408, 10.1029/2000jd900841, 2001.
Jung, J. G., Adams, P. J., and Pandis, S. N.: Simulating the size distribution and chemical composition of ultrafine particles during nucleation events, Atmospheric Environment, 40, 2248-2259, 2006.

Jung, J. G., Fountoukis, C., Adams, P. J., and Pandis, S. N.: Simulation of in situ ultrafine particle formation in the eastern United States using PMCAMx-UF, J. Geophys. Res.-Atmos., 115, D03203, doi: 10.1029/2009jd012313, 2010.
Kahn, R. A., Gaitley, B. J., Martonchik, J. V., Diner, D. J., Crean, K. A., and Holben, B.: Multiangle Imaging Spectroradiometer (MISR) global aerosol optical depth validation based on 2 years of coincident Aerosol Robotic Network (AERONET) observations, J. Geophys. Res.-Atmos., 110, D10s04
10.1029/2004jd004706, 2005.
Kettle, A. J., Andreae, M. O., Amouroux, D., Andreae, T. W., Bates, T. S., Berresheim, H., Bingemer, H., Boniforti, R., Curran, M. A. J., DiTullio, G. R., Helas, G., Jones, G. B., Keller, M. D., Kiene, R. P., Leck, C., Levasseur, M., Malin, G., Maspero, M., Matrai, P., McTaggart, A. R., Mihalopoulos, N., Nguyen, B. C., Novo, A., Putaud, J. P., Rapsomanikis, S., Roberts, G., Schebeske, G., Sharma, S., Simo, R., Staubes, R., Turner, S., and Uher, G.: A global database of sea surface dimethylsulfide (DMS) measurements and a procedure to predict sea surface DMS as a function of latitude, longitude, and month, Global Biogeochemical Cycles, 13, 399-444, 10.1029/1999gb900004, 1999.
Kettle, A. J., and Andreae, M. O.: Flux of dimethylsulfide from the oceans: A comparison of updated data sets and flux models, Journal of Geophysical Research: Atmospheres, 105, 26793-26808, 10.1029/2000JD900252, 2000.
Koch, D., Jacob, D., Tegen, I., Rind, D., and Chin, M.: Tropospheric sulfur simulation and sulfate direct radiative forcing in the Goddard Institute for Space Studies general circulation model, J. Geophys. Res.-Atmos., 104, 23799-23822, 10.1029/1999jd900248, 1999.
Koch, D., Schmidt, G. A., and Field, C. V.: Sulfur, sea salt, and radionuclide aerosols in GISS ModelE, J. Geophys. Res.-Atmos., 111, D06206, doi:10.1029/2004jd005550, 2006.
Koch, D., Bond, T. C., Streets, D., Unger, N., and van der Werf, G. R.: Global impacts of aerosols from particular source regions and sectors, J. Geophys. Res.-Atmos., 112, D02205, doi: 10.1029/2005jd007024, 2007.
Koch, D., Bauer, S. E., Del Genio, A., Faluvegi, G., McConnell, J. R., Menon, S., Miller, R. L., Rind, D., Ruedy, R., Schmidt, G. A., and Shindell, D.: Coupled Aerosol-Chemistry-Climate Twentieth-Century Transient Model Investigation: Trends in Short-Lived Species and Climate Responses, J Climate, 24, 2693-2714, 10.1175/2011jcli3582.1, 2011.
Korhonen, H., Carslaw, K. S., Spracklen, D. V., Mann, G. W., and Woodhouse, M. T.: Influence of oceanic dimethyl sulfide emissions on cloud condensation nuclei concentrations and seasonality over the remote Southern Hemisphere oceans: A global model study, J. Geophys. Res.-Atmos., 113, D15204, doi: 10.1029/2007jd009718, 2008.
Lamarque, J.-F., Shindell, D. T., Josse, B., Eyring, V., Young, P. J., Cionni, I., Bergmann, D., Cameron-Smith, P., Collins, W. J., Doherty, R., Dalsoren, S., Faluvegi, G., Folberth, G., Ghan, S. J., Horowitz, L. W., Lee, Y. H., McKenzie, I., Nagashima, T., Naik, V., Plummer, D., Rumbold, S., Skeie, R., Stevenson, D. S., Strode, S., Sudo, K., Szopa, S., Voulgarakis, A., and Zeng, G.: The Atmospheric Chemistry and Climate Model Intercomparison Project (ACCMIP): Overview and description of models, simulations and climate diagnostics, Geoscientific Model Development, accepted, 2012.
Lamarque, J. F., Dentener, F., McConnell, J., Ro, C. U., Shaw, M., Vet, R., Bergmann, D., Cameron-Smith, P., Dalsoren, S., Doherty, R., Faluvegi, G., Ghan, S. J., Josse, B.,

Lee, Y. H., MacKenzie, I. A., Plummer, D., Shindell, D. T., Skeie, R. B., Stevenson, D. S., Strode, S., Zeng, G., Curran, M., Dahl-Jensen, D., Das, S., Fritzsche, D., and Nolan, M.: Multi-model mean nitrogen and sulfur deposition from the Atmospheric Chemistry and Climate Model Intercomparison Project (ACCMIP): evaluation of historical and projected future changes, Atmospheric Chemistry and Physics, 13, 7997-8018, 2013a.
Lamarque, J. F., Shindell, D. T., Josse, B., Young, P. J., Cionni, I., Eyring, V., Bergmann, D., Cameron-Smith, P., Collins, W. J., Doherty, R., Dalsoren, S., Faluvegi, G., Folberth, G., Ghan, S. J., Horowitz, L. W., Lee, Y. H., MacKenzie, I. A., Nagashima, T., Naik, V., Plummer, D., Righi, M., Rumbold, S. T., Schulz, M., Skeie, R. B., Stevenson, D. S., Strode, S., Sudo, K., Szopa, S., Voulgarakis, A., and Zeng, G.: The Atmospheric Chemistry and Climate Model Intercomparison Project (ACCMIP): overview and description of models, simulations and climate diagnostics, Geoscientific Model Development, 6, 179-206, 10.5194/gmd-6-179-2013, 2013b.
Lauer, A., Hendricks, J., Ackermann, I., Schell, B., Hass, H., and Metzger, S.: Simulating aerosol microphysics with the ECHAM/MADE GCM - Part I: Model description and comparison with observations, Atmospheric Chemistry and Physics, 5, 3251-3276, 2005.
Lee, Y. H., Chen, K., and Adams, P. J.: Development of a global model of mineral dust aerosol microphysics, Atmospheric Chemistry and Physics, 9, 2441-2458, 2009.
Lee, Y. H., and Adams, P. J.: Evaluation of aerosol distributions in the GISS-TOMAS global aerosol microphysics model with remote sensing observations, Atmospheric Chemistry and Physics, 10, 2129-2144, 2010.
Lee, Y. H., and Adams, P. J.: A Fast and Efficient Version of the TwO-Moment Aerosol Sectional (TOMAS) Global Aerosol Microphysics Model, Aerosol Science and Technology, 46, 678-689, 10.1080/02786826.2011.643259, 2012.
Lee, Y. H., Lamarque, J. F., Flanner, M. G., Jiao, C., Shindell, D. T., Berntsen, T., Bisiaux, M. M., Cao, J., Collins, W. J., Curran, M., Edwards, R., Faluvegi, G., Ghan, S., Horowitz, L. W., McConnell, J. R., Ming, J., Myhre, G., Nagashima, T., Naik, V., Rumbold, S. T., Skeie, R. B., Sudo, K., Takemura, T., Thevenon, F., Xu, B., and Yoon, J. H.: Evaluation of preindustrial to present-day black carbon and its albedo forcing from Atmospheric Chemistry and Climate Model Intercomparison Project (ACCMIP), Atmospheric Chemistry and Physics, 13, 2607-2634, 10.5194/acp-13-2607-2013, 2013a.
Lee, Y. H., Pierce, J. R., and Adams, P. J.: Representation of nucleation mode microphysics in a global aerosol model with sectional microphysics, Geoscientific Model Development, 6, 1221-1232, 2013b.
Liss, P. S., and Merlivat, L.: Air-sea gas exchange rates: Introduction and synthesis, The Role of Air-Sea Exchange in Geochemical Cycling, Springer, New York, 1986.
Liu, X. H., Penner, J. E., and Herzog, M.: Global modeling of aerosol dynamics: Model description, evaluation, and interactions between sulfate and nonsulfate aerosols, J. Geophys. Res.-Atmos., 110, D18206, doi: 10.1029/2004jd005674, 2005.
Lohmann, U., and Feichter, J.: Global indirect aerosol effects: a review, Atmospheric Chemistry and Physics, 5, 715-737, 2005.
Mahowald, N. M., Engelstaedter, S., Luo, C., Sealy, A., Artaxo, P., Benitez-Nelson, C., Bonnet, S., Chen, Y., Chuang, P. Y., Cohen, D. D., Dulac, F., Herut, B., Johansen, A. M., Kubilay, N., Losno, R., Maenhaut, W., Paytan, A., Prospero, J. A., Shank, L. M., and Siefert, R. L.: Atmospheric Iron Deposition: Global Distribution, Variability, and Human

Perturbations, in: Annual Review of Marine Science, Annual Review of Marine Science, 245-278, 2009.
Mann, G. W., Carslaw, K. S., Spracklen, D. V., Ridley, D. A., Manktelow, P. T., Chipperfield, M. P., Pickering, S. J., and Johnson, C. E.: Description and evaluation of GLOMAP-mode: a modal global aerosol microphysics model for the UKCA composition-climate model, Geoscientific Model Development, 3, 519-551, 10.5194/gmd-3-519-2010, 2010.
Menon, S., Del Genio, A. D., Koch, D., and Tselioudis, G.: GCM Simulations of the aerosol indirect effect: Sensitivity to cloud parameterization and aerosol burden, Journal of the Atmospheric Sciences, 59, 692-713, 10.1175/1520-0469(2002)059<0692:gsotai>2.0.co;2, 2002.
Menon, S., Del Genio, A. D., Kaufman, Y., Bennartz, R., Koch, D., Loeb, N., and Orlikowski, D.: Analyzing signatures of aerosol-cloud interactions from satellite retrievals and the GISS GCM to constrain the aerosol indirect effect, J. Geophys. Res.-Atmos., 113, D14s22 10.1029/2007jd009442, 2008.
Merikanto, J., Spracklen, D. V., Mann, G. W., Pickering, S. J., and Carslaw, K. S.: Impact of nucleation on global CCN, Atmospheric Chemistry and Physics, 9, 8601-8616, 2009.
Miller, R. L., Cakmur, R. V., Perlwitz, J., Geogdzhayev, I. V., Ginoux, P., Koch, D., Kohfeld, K. E., Prigent, C., Ruedy, R., Schmidt, G. A., and Tegen, I.: Mineral dust aerosols in the NASA goddard institute for Space Sciences ModelE atmospheric general circulation model, J. Geophys. Res.-Atmos., 111, D06208, doi: 10.1029/2005jd005796, 2006.
Mishchenko, M. I., Travis, L. D., and Mackowski, D. W.: T-matrix computations of light scattering by nonspherical particles: A review, Journal of Quantitative Spectroscopy & Radiative Transfer, 55, 535-575, 10.1016/0022-4073(96)00002-7, 1996.
Monahan, E. C., Spiel, D. E., and David, K. L.: A model of marine aerosol generation via whitecaps and wave disruption, in Oceanic Whitecaps, edited by: Monahan, E. C., and Mac Niocaill, G., Oceanographic Sciences Library, 167–174 pp., 1986.
Myhre, G., Samset, B. H., Schulz, M., Balkanski, Y., Bauer, S., Berntsen, T. K., Bian, H., Bellouin, N., Chin, M., Diehl, T., Easter, R. C., Feichter, J., Ghan, S. J., Hauglustaine, D., Iversen, T., Kinne, S., Kirkev√•g, A., Lamarque, J. F., Lin, G., Liu, X., Lund, M. T., Luo, G., Ma, X., van Noije, T., Penner, J. E., Rasch, P. J., Ruiz, A., Seland, ò., Skeie, R. B., Stier, P., Takemura, T., Tsigaridis, K., Wang, P., Wang, Z., Xu, L., Yu, H., Yu, F., Yoon, J. H., Zhang, K., Zhang, H., and Zhou, C.: Radiative forcing of the direct aerosol effect from AeroCom Phase II simulations, Atmos. Chem. Phys., 13, 1853-1877, 10.5194/acp-13-1853-2013, 2013a.
Myhre, G., Shindell, D., Brèon, F.-M., Collins, W., Fuglestvedt, J., Huang, J., Koch, D., Lamarque, J. F., Lee, D., Mendoza, B., Nakajima, T., Robock, A., Stephens, G., Takemura, T., and Zhang, H.: Anthropogenic and Natural Radiative Forcing. In: Climate Change 2013: The Physical Science Basis. , Contribution of Working Group I to the Fifth Assessment
Report of the Intergovernmental Panel on Climate Change, Cambridge University Press. Cambridge, United Kingdom and New York, NY, USA, 2013b.

Nabat, P., Somot, S., Mallet, M., Chiapello, I., Morcrette, J. J., Solmon, F., Szopa, S., Dulac, F., Collins, W., Ghan, S., Horowitz, L. W., Lamarque, J. F., Lee, Y. H., Naik, V., Nagashima, T., Shindell, D., and Skeie, R.: A 4-D climatology (1979-2009) of the monthly tropospheric aerosol optical depth distribution over the Mediterranean region from a comparative evaluation and blending of remote sensing and model products, Atmospheric Measurement Techniques, 6, 1287-1314, 10.5194/amt-6-1287-2013, 2013.

Naik, V., Voulgarakis, A., Fiore, A. M., Horowitz, L. W., Lamarque, J. F., Lin, M., Prather, M. J., Young, P. J., Bergmann, D., Cameron-Smith, P. J., Cionni, I., Collins, W. J., Dalsoren, S. B., Doherty, R., Eyring, V., Faluvegi, G., Folberth, G. A., Josse, B., Lee, Y. H., MacKenzie, I. A., Nagashima, T., van Noije, T. P. C., Plummer, D. A., Righi, M., Rumbold, S. T., Skeie, R., Shindell, D. T., Stevenson, D. S., Strode, S., Sudo, K., Szopa, S., and Zeng, G.: Preindustrial to present-day changes in tropospheric hydroxyl radical and methane lifetime from the Atmospheric Chemistry and Climate Model Intercomparison Project (ACCMIP), Atmospheric Chemistry and Physics, 13, 5277-5298, 10.5194/acp-13-5277-2013, 2013.

Napari, I., Noppel, M., Vehkamaki, H., and Kulmala, M.: Parametrization of ternary nucleation rates for H2SO4-NH3-H2O vapors, J. Geophys. Res.-Atmos., 107, 4381, doi: 10.1029/2002JD002132, 2002.

Nenes, A., Pandis, S. N., and Pilinis, C.: ISORROPIA: A New Thermodynamic Equilibrium Model for Multiphase Multicomponent Inorganic Aerosols, Aquatic Geochemistry, 4, 123-152, 10.1023/A:1009604003981, 1998.

Nguyen, B. C., Mihalopoulos, N., Putaud, J. P., Gaudry, A., Gallet, L., Keene, W. C., and Galloway, J. N.: COVARIATIONS IN OCEANIC DIMETHYL SULFIDE, ITS OXIDATION-PRODUCTS AND RAIN ACIDITY AT AMSTERDAM ISLAND IN THE SOUTHERN INDIAN-OCEAN, Journal of Atmospheric Chemistry, 15, 39-53, 10.1007/bf00053608, 1992.

Nightingale, P. D., Malin, G., Law, C. S., Watson, A. J., Liss, P. S., Liddicoat, M. I., Boutin, J., and Upstill-Goddard, R. C.: In situ evaluation of air-sea gas exchange parameterizations using novel conservative and volatile tracers, Global Biogeochemical Cycles, 14, 373-387, 10.1029/1999gb900091, 2000.

Petzold, A., Fiebig, M., Flentje, H., Keil, A., Leiterer, U., Schroder, F., Stifter, A., Wendisch, M., and Wendling, P.: Vertical variability of aerosol properties observed at a continental site during the Lindenberg Aerosol Characterization Experiment (LACE 98), J. Geophys. Res.-Atmos., 107, 8128, 8128, doi: 10.1029/2001jd001043, 2002.

Pierce, J. R., and Adams, P. J.: Global evaluation of CCN formation by direct emission of sea salt and growth of ultrafine sea salt, J. Geophys. Res.-Atmos., 111, D06203, doi:10.1029/2005JD006186, 2006.

Pierce, J. R., Chen, K., and Adams, P. J.: Contribution of primary carbonaceous aerosol to cloud condensation nuclei: processes and uncertainties evaluated with a global aerosol microphysics model, Atmospheric Chemistry and Physics, 7, 5447-5466, 2007.

Pierce, J. R., and Adams, P. J.: A Computationally Efficient Aerosol Nucleation/Condensation Method: Pseudo-Steady-State Sulfuric Acid, Aerosol Science and Technology, 43, 216-226, 2009a.

Pierce, J. R., and Adams, P. J.: Uncertainty in global CCN concentrations from uncertain aerosol nucleation and primary emission rates, Atmospheric Chemistry and Physics, 9, 1339-1356, 2009b.

Prather, M. J.: Numerical Advection by Conservation of 2nd-Order Moments, J. Geophys. Res.-Atmos., 91, 6671-6681, 1986.
Prospero, J. M., and Bonatti, E.: CONTINENTAL DUST IN ATMOSPHERE OF EASTERN EQUATORIAL PACIFIC, Journal of Geophysical Research, 74, 3362-3371, doi: 10.1029/JC074i013p03362, 1969.
Prospero, J. M., Bullard, J. E., and Hodgkins, R.: High-Latitude Dust Over the North Atlantic: Inputs from Icelandic Proglacial Dust Storms, Science, 335, 1078-1082, 10.1126/science.1217447, 2012.
Putaud, J. P.: A European aerosol phenomenology; physical and chemical characteristics of particulate matter at kerbside, urban, rural and background sites in Europe, European Commission, EUR 20411 EN, 2003.
Putaud, J. P., Van Dingenen, R., Alastuey, A., Bauer, H., Birmili, W., Cyrys, J., Flentje, H., Fuzzi, S., Gehrig, R., Hansson, H. C., Harrison, R. M., Herrmann, H., Hitzenberger, R., Hueglin, C., Jones, A. M., Kasper-Giebl, A., Kiss, G., Kousa, A., Kuhlbusch, T. A. J., Loeschau, G., Maenhaut, W., Molnar, A., Moreno, T., Pekkanen, J., Perrino, C., Pitz, M., Puxbaum, H., Querol, X., Rodriguez, S., Salma, I., Schwarz, J., Smolik, J., Schneider, J., Spindler, G., ten Brink, H., Tursic, J., Viana, M., Wiedensohler, A., and Raes, F.: A European aerosol phenomenology-3: Physical and chemical characteristics of particulate matter from 60 rural, urban, and kerbside sites across Europe, Atmospheric Environment, 44, 1308-1320, 10.1016/j.atmosenv.2009.12.011, 2010.
Raper, J. L., Kleb, M. M., Jacob, D. J., Davis, D. D., Newell, R. E., Fuelberg, H. E., Bendura, R. J., Hoell, J. M., and McNeal, R. J.: Pacific Exploratory Mission in the tropical Pacific: PEM-Tropics B, March-April 1999, J. Geophys. Res.-Atmos., 106, 32401-32425, 10.1029/2000jd900833, 2001.
Remer, L. A., Kleidman, R. G., Levy, R. C., Kaufman, Y. J., Tanre, D., Mattoo, S., Martins, J. V., Ichoku, C., Koren, I., Yu, H., and Holben, B. N.: Global aerosol climatology from the MODIS satellite sensors, J. Geophys. Res.-Atmos., 113, D14s07 10.1029/2007jd009661, 2008.
Rienecker, M. M., Suarez, M. J., Gelaro, R., Todling, R., Bacmeister, J., Liu, E., Bosilovich, M. G., Schubert, S. D., Takacs, L., Kim, G.-K., Bloom, S., Chen, J., Collins, D., Conaty, A., da Silva, A., Gu, W., Joiner, J., Koster, R. D., Lucchesi, R., Molod, A., Owens, T., Pawson, S., Pegion, P., Redder, C. R., Reichle, R., Robertson, F. R., Ruddick, A. G., Sienkiewicz, M., and Woollen, J.: MERRA: NASA's Modern-Era Retrospective Analysis for Research and Applications, J Climate, 24, 3624-3648, 10.1175/JCLI-D-11-00015.1, 2011.
Savoie, D. L., and Prospero, J. M.: COMPARISON OF OCEANIC AND CONTINENTAL SOURCES OF NON-SEA-SALT SULFATE OVER THE PACIFIC-OCEAN, Nature, 339, 685-687, 10.1038/339685a0, 1989.
Schmidt, G. A., Ruedy, R., Hansen, J. E., Aleinov, I., Bell, N., Bauer, M., Bauer, S., Cairns, B., Canuto, V., Cheng, Y., Del Genio, A., Faluvegi, G., Friend, A. D., Hall, T. M., Hu, Y. Y., Kelley, M., Kiang, N. Y., Koch, D., Lacis, A. A., Lerner, J., Lo, K. K., Miller, R. L., Nazarenko, L., Oinas, V., Perlwitz, J., Perlwitz, J., Rind, D., Romanou, A., Russell, G. L., Sato, M., Shindell, D. T., Stone, P. H., Sun, S., Tausnev, N., Thresher, D., and Yao, M. S.: Present-day atmospheric simulations using GISS ModelE: Comparison to in situ, satellite, and reanalysis data, J Climate, 19, 153-192, 10.1175/jcli3612.1, 2006.

Schmidt, G. A., Kelley, M., Nazarenko, L., Ruedy, R., Russell, G. L., Aleinov, I., Bauer, M., Bauer, S. E., Bhat, M. K., Bleck, R., Canuto, V., Chen, Y.-H., Cheng, Y., Clune, T. L., Del Genio, A., de Fainchtein, R., Faluvegi, G., Hansen, J. E., Healy, R. J., Kiang, N. Y., Koch, D., Lacis, A. A., LeGrande, A. N., Lerner, J., Lo, K. K., Matthews, E. E., Menon, S., Miller, R. L., Oinas, V., Oloso, A. O., Perlwitz, J. P., Puma, M. J., Putman, W. M., Rind, D., Romanou, A., Sato, M., Shindell, D. T., Sun, S., Syed, R. A., Tausnev, N., Tsigaridis, K., Unger, N., Voulgarakis, A., Yao, M.-S., and Zhang, J.: Configuration and assessment of the GISS ModelE2 contributions to the CMIP5 archive, Journal of Advances in Modeling Earth Systems, 6, 141-184, 10.1002/2013ms000265, 2014.

Seinfeld, J. H., and Pandis, S. N.: Atmospheric Chemistry and Physics, John Wiley and Sons, New York, 1998.

Shindell, D., Faluvegi, G., Walsh, M., Anenberg, S. C., Van Dingenen, R., Muller, N. Z., Austin, J., Koch, D., and Milly, G.: Climate, health, agricultural and economic impacts of tighter vehicle-emission standards, Nature Climate Change, 1, 59-66, 10.1038/nclimate1066, 2011.

Shindell, D. T., Faluvegi, G., Unger, N., Aguilar, E., Schmidt, G. A., Koch, D. M., Bauer, S. E., and Miller, R. L.: Simulations of preindustrial, present-day, and 2100 conditions in the NASA GISS composition and climate model G-PUCCINI, Atmospheric Chemistry and Physics, 6, 4427-4459, 2006.

Shindell, D. T., Lamarque, J. F., Schulz, M., Flanner, M., Jiao, C., Chin, M., Young, P. J., Lee, Y. H., Rotstayn, L., Mahowald, N., Milly, G., Faluvegi, G., Balkanski, Y., Collins, W. J., Conley, A. J., Dalsoren, S., Easter, R., Ghan, S., Horowitz, L., Liu, X., Myhre, G., Nagashima, T., Naik, V., Rumbold, S. T., Skeie, R., Sudo, K., Szopa, S., Takemura, T., Voulgarakis, A., Yoon, J. H., and Lo, F.: Radiative forcing in the ACCMIP historical and future climate simulations, Atmospheric Chemistry and Physics, 13, 2939-2974, 10.5194/acp-13-2939-2013, 2013.

Sihto, S. L., Kulmala, M., Kerminen, V. M., Dal Maso, M., Petaja, T., Riipinen, I., Korhonen, H., Arnold, F., Janson, R., Boy, M., Laaksonen, A., and Lehtinen, K. E. J.: Atmospheric sulphuric acid and aerosol formation: implications from atmospheric measurements for nucleation and early growth mechanisms, Atmospheric Chemistry and Physics, 6, 4079-4091, 2006.

Singh, S., Adams, P. J., Misquitta, A., Lee, K. J., Lipsky, E. M., and Robinson, A. L.: Computational Analysis of Particle Nucleation in Dilution Tunnels: Effects of Flow Configuration and Tunnel Geometry, Aerosol Science and Technology, 48, 638-648, 10.1080/02786826.2014.910291, 2014.

Spracklen, D. V., Pringle, K. J., Carslaw, K. S., Chipperfield, M. P., and Mann, G. W.: A global off-line model of size-resolved aerosol microphysics: I. Model development and prediction of aerosol properties, Atmospheric Chemistry and Physics, 5, 2227-2252, 2005.

Spracklen, D. V., Carslaw, K. S., Merikanto, J., Mann, G. W., Reddington, C. L., Pickering, S., Ogren, J. A., Andrews, E., Baltensperger, U., Weingartner, E., Boy, M., Kulmala, M., Laakso, L., Lihavainen, H., Kivekas, N., Komppula, M., Mihalopoulos, N., Kouvarakis, G., Jennings, S. G., O'Dowd, C., Birmili, W., Wiedensohler, A., Weller, R., Gras, J., Laj, P., Sellegri, K., Bonn, B., Krejci, R., Laaksonen, A., Hamed, A., Minikin, A., Harrison, R. M., Talbot, R., and Sun, J.: Explaining global surface aerosol number

concentrations in terms of primary emissions and particle formation, Atmospheric Chemistry and Physics, 10, 4775-4793, 10.5194/acp-10-4775-2010, 2010.
Spracklen, D. V., Carslaw, K. S., Poeschl, U., Rap, A., and Forster, P. M.: Global cloud condensation nuclei influenced by carbonaceous combustion aerosol, Atmospheric Chemistry and Physics, 11, 9067-9087, 10.5194/acp-11-9067-2011, 2011.
Stevens, R. G., Pierce, J. R., Brock, C. A., Reed, M. K., Crawford, J. H., Holloway, J. S., Ryerson, T. B., Huey, L. G., and Nowak, J. B.: Nucleation and growth of sulfate aerosol in coal-fired power plant plumes: sensitivity to background aerosol and meteorology, Atmos. Chem. Phys., 12, 189-206, 10.5194/acp-12-189-2012, 2012.
Stevenson, D. S., Young, P. J., Naik, V., Lamarque, J. F., Shindell, D. T., Voulgarakis, A., Skeie, R. B., Dalsoren, S. B., Myhre, G., Berntsen, T. K., Folberth, G. A., Rumbold, S. T., Collins, W. J., MacKenzie, I. A., Doherty, R. M., Zeng, G., van Noije, T. P. C., Strunk, A., Bergmann, D., Cameron-Smith, P., Plummer, D. A., Strode, S. A., Horowitz, L., Lee, Y. H., Szopa, S., Sudo, K., Nagashima, T., Josse, B., Cionni, I., Righi, M., Eyring, V., Conley, A., Bowman, K. W., Wild, O., and Archibald, A.: Tropospheric ozone changes, radiative forcing and attribution to emissions in the Atmospheric Chemistry and Climate Model Intercomparison Project (ACCMIP), Atmospheric Chemistry and Physics, 13, 3063-3085, 10.5194/acp-13-3063-2013, 2013.
Stier, P., Feichter, J., Kinne, S., Kloster, S., Vignati, E., Wilson, J., Ganzeveld, L., Tegen, I., Werner, M., Balkanski, Y., Schulz, M., Boucher, O., Minikin, A., and Petzold, A.: The aerosol-climate model ECHAM5-HAM, Atmospheric Chemistry and Physics, 5, 1125-1156, 2005.
Tegen, I., Harrison, S. P., Kohfeld, K., Prentice, I. C., Coe, M., and Heimann, M.: Impact of vegetation and preferential source areas on global dust aerosol: Results from a model study, J. Geophys. Res.-Atmos., 107, 4576, 4576, doi: 10.1029/2001jd000963, 2002.
Textor, C., Schulz, M., Guibert, S., Kinne, S., Balkanski, Y., Bauer, S., Berntsen, T., Berglen, T., Boucher, O., Chin, M., Dentener, F., Diehl, T., Easter, R., Feichter, H., Fillmore, D., Ghan, S., Ginoux, P., Gong, S., Kristjansson, J. E., Krol, M., Lauer, A., Lamarque, J. F., Liu, X., Montanaro, V., Myhre, G., Penner, J., Pitari, G., Reddy, S., Seland, O., Stier, P., Takemura, T., and Tie, X.: Analysis and quantification of the diversities of aerosol life cycles within AeroCom, Atmospheric Chemistry and Physics, 6, 1777-1813, 2006.
Thornton, D. C., Bandy, A. R., Blomquist, B. W., Driedger, A. R., and Wade, T. P.: Sulfur dioxide distribution over the Pacific Ocean 1991–1996, Journal of Geophysical Research: Atmospheres, 104, 5845-5854, 10.1029/1998JD100048, 1999.
Trivitayanurak, W., Adams, P. J., Spracklen, D. V., and Carslaw, K. S.: Tropospheric aerosol microphysics simulation with assimilated meteorology: model description and intermodel comparison, Atmospheric Chemistry and Physics, 8, 3149-3168, 2008.
Tsigaridis, K., and Kanakidou, M.: Secondary organic aerosol importance in the future atmosphere, Atmospheric Environment, 41, 4682-4692, 10.1016/j.atmosenv.2007.03.045, 2007.
Tsigaridis, K., Koch, D., and Menon, S.: Uncertainties and importance of sea spray composition on aerosol direct and indirect effects, J. Geophys. Res.-Atmos., 118, 220-235, 10.1029/2012jd018165, 2013.

Tzivion, S., Feingold, G., and Levin, Z.: An Efficient Numerical Solution to the Stochastic Collection Equation, Journal of the Atmospheric Sciences, 44, 3139-3149, 1987.
Tzivion, S., Feingold, G., and Levin, Z.: THE EVOLUTION OF RAINDROP SPECTRA .2. COLLISIONAL COLLECTION BREAKUP AND EVAPORATION IN A RAINSHAFT, Journal of the Atmospheric Sciences, 46, 3312-3327, 10.1175/1520-0469(1989)046<3312:teorsp>2.0.co;2, 1989.
Tzivion, S., Reisin, T. G., and Levin, Z.: A new formulation of the spectral multi-moment method for calculating the kinetic collection equation: More accuracy with fewer bins, Journal of Computational Physics, 171, 418-422, 10.1006/jcph.2001.6776, 2001.
Uematsu, M., Duce, R. A., and Prospero, J. M.: DEPOSITION OF ATMOSPHERIC MINERAL PARTICLES IN THE NORTH PACIFIC-OCEAN, Journal of Atmospheric Chemistry, 3, 123-138, 10.1007/bf00049372, 1985.
van der Werf, G. R., Randerson, J. T., Giglio, L., Collatz, G. J., Mu, M., Kasibhatla, P. S., Morton, D. C., DeFries, R. S., Jin, Y., and van Leeuwen, T. T.: Global fire emissions and the contribution of deforestation, savanna, forest, agricultural, and peat fires (1997-2009), Atmospheric Chemistry and Physics, 10, 11707-11735, 10.5194/acp-10-11707-2010, 2010.
Vehkamaki, H., Kulmala, M., Napari, I., Lehtinen, K. E. J., Timmreck, C., Noppel, M., and Laaksonen, A.: An improved parameterization for sulfuric acid-water nucleation rates for tropospheric and stratospheric conditions, J. Geophys. Res.-Atmos., 107, 4622, DOI: 10.1029/2002JD002184, 2002.
Vignati, E., Wilson, J., and Stier, P.: M7: An efficient size-resolved aerosol microphysics module for large-scale aerosol transport models, J. Geophys. Res.-Atmos., 109, D22202, doi:10.1029/2003jd004485, 2004.
Wang, M., Ghan, S., Ovchinnikov, M., Liu, X., Easter, R., Kassianov, E., Qian, Y., and Morrison, H.: Aerosol indirect effects in a multi-scale aerosol-climate model PNNL-MMF, Atmospheric Chemistry and Physics, 11, 5431-5455, 10.5194/acp-11-5431-2011, 2011.
Wanninkhof, R.: Relationship between wind speed and gas exchange over the ocean, Journal of Geophysical Research: Oceans, 97, 7373-7382, 10.1029/92jc00188, 1992.
Westervelt, D. M., Pierce, J. R., Riipinen, I., Trivitayanurak, W., Hamed, A., Kulmala, M., Laaksonen, A., Decesari, S., and Adams, P. J.: Formation and growth of nucleated particles into cloud condensation nuclei: model–measurement comparison, Atmos. Chem. Phys., 13, 7645-7663, 10.5194/acp-13-7645-2013, 2013.
Young, P. J., Archibald, A. T., Bowman, K. W., Lamarque, J. F., Naik, V., Stevenson, D. S., Tilmes, S., Voulgarakis, A., Wild, O., Bergmann, D., Cameron-Smith, P., Cionni, I., Collins, W. J., Dalsoren, S. B., Doherty, R. M., Eyring, V., Faluvegi, G., Horowitz, L. W., Josse, B., Lee, Y. H., MacKenzie, I. A., Nagashima, T., Plummer, D. A., Righi, M., Rumbold, S. T., Skeie, R. B., Shindell, D. T., Strode, S. A., Sudo, K., Szopa, S., and Zeng, G.: Pre-industrial to end 21st century projections of tropospheric ozone from the Atmospheric Chemistry and Climate Model Intercomparison Project (ACCMIP), Atmospheric Chemistry and Physics, 13, 2063-2090, 10.5194/acp-13-2063-2013, 2013.
Yu, F., and Luo, G.: Simulation of particle size distribution with a global aerosol model: contribution of nucleation to aerosol and CCN number concentrations, Atmospheric Chemistry and Physics, 9, 7691-7710, 2009.

Zhang, Y., Seigneur, C., Seinfeld, J. H., Jacobson, M. Z., and Binkowski, F. S.: Simulation of aerosol dynamics: A comparative review of algorithms used in air quality models, Aerosol Science and Technology, 31, 487-514, 1999.

Table 1. Aerosol and precursor gas emissions used in ModelE2-TOMAS and ModelE2-OMA and the nucleation scheme used in the ModelE2-TOMAS simulations

Emission/Process	TOMAS model	Bulk model
Anthropogenic emissions	CMIP5 2000 emissions (Lamarque et al., 2012)	CMIP5 2000 emissions (Lamarque et al., 2012)
Biomass burning emissions	Climatological-average GFED3 emissions from 1997 to 2009 (van der Werf et al., 2010)	Climatological-average GFED3 emissions from 1997 to 2009 (van der Werf et al., 2010)
Primary sulfate emission assumption	1.0% of total sulfur emissions	2.5% of total sulfur emissions
DMS emission	Seawater DMS concentrations from Kettle et al. (1999) Sea-to-air transfer function from Liss and Merlivat (1986)	Seawater DMS concentrations from Kettle et al. (1999) Sea-to-air transfer function from Nightingale et al. (2000)
Sea-salt emission	Gong et al. (2002); the upper diameter limit of 10 um	Gong et al. (2002); the upper diameter limit of 8 um
Dust emission	See text for the details; the upper size diameter of 10 um	See text for the details; the upper size diameter of 16 um
Nucleation	Three nucleation cases 1. BASE - Binary nucleation 2. LowNUC - Binary nucleation with 5 times lower sulfuric acid concentrations 3. NoNUC – no nucleation	N/A

Table 2. Emission size distributions assumed in ModelE2-TOMAS. *This is the soil size assumption used in ModelE2-TOMAS, and the dust emission size distribution is additionally influenced by meteorological variables. GMD stands for geometric mean diameter, and GSD for geometric standard deviation.

Species	Emissions	Size assumptions
Sulfate	All emissions	Bimodal distribution GMD=10nm, GSD=1.6 (5% of total mass) GMD=70 nm, GSD=2.0 (95% of total mass)
EC and OC	Fossil fuel and Biofuel Biomass burning	GMD=60 nm, GSD=1.59 GMD=150 nm, GSD=1.59
Dust*	Clay Silt	GMD=140 nm, GSD=2.0 GMD=1.15 μm, GSD=2.0

Table 3. Global budgets for DMS and SO_2 from the BASE run in ModelE2-TOMAS and ModelE2-OMA. The ModelE2-TOMAS values are presented before slash and the ModelE2-OMA values are after slash. Values in parentheses are ranges from other global models including Wang et al. (2011), Liu et al. (2005), and those listed in Liu et al. (2005).

	DMS	SO2
Burden [Tg S]	0.05 / 0.11 (0.02-0.15)	0.36 / 0.38 (0.2-0.69)
Total source [Tg S yr^{-1}]	16.1 / 28.7	80 / 90
Emission	16.1/ 28.7 (10.7-23.7)	65.6 / 64.7 (61.2-92.0)
Chemistry	-	14.4 / 25.3
Sink [Tg S yr^{-1}]	16.1/ 28.7	80 / 89
Gas-phase oxidation	16.1/ 28.7	12.3 / 14.6 (6.1-22.0)
Aqueous-phase oxidation	-	30.8 / 35.8 (24.5-57.8)
Wet deposition	-	0.36 / 0.4 (0-19.9)
Dry deposition	-	37 / 38.8 (15.78-55)
Lifetime [days]	1.2 / 1.5 (0.5-3.0)	1.9 / 1.5 (0.6-2.6)

Table 4. Global aerosol budgets of the BASE run in ModelE2-TOMAS. Values in the parentheses are the mean and normalized standard deviations obtained from Table 10 in Textor et al. (2006). The mass budgets for sulfate are presented as Tg S.

	Sulfate	Elemental carbon (EC)	Organic matter (OM)	Sea-salt	Dust
Burden [Tg]	0.67	0.19	1.2	3.6	9.1
Total source [Tg yr^{-1}]	43.7	7.4	60.8	3231.9	705.8
Emission	0.66	7.4	43.7	3231.9	705.8
Wet deposition [Tg yr^{-1}]	42.9	7.1	59.1	1046.9	336.8
By convective clouds [%]	27	24	24	54	29
Dry deposition [Tg yr^{-1}]	0.8	0.3	1.6	2184.9	369.9
Lifetime [days]	5.6 (4.1, 18%)	9.6 (7.1, 33%)	7.2 (6.5, 27%)	0.4 (0.5, 58%)	4.7 (4.1, 43%)
Removal rate coefficient [day^{-1}]	0.18 (0.25, 18%)	0.1 (0.15, 21%)	0.14 (0.16, 24%)	2.4 (5.1, 188%)	0.21 (0.31, 62%)
Wet deposition	0.18 (0.22, 22%)	0.1 (0.12, 31%)	0.14 (0.14, 32%)	0.79 (0.79, 77%)	0.1 (0.08, 42%)
Dry deposition	0.0032 (0.03, 55%)	0.004 (0.03, 55%)	0.0037 (0.03, 49%)	1.6 (4.3, 219%)	0.11 (0.23, 84%)
Wet/(Wet+Dry) [%]	98 (89, 8%)	96 (79, 17%)	97 (80, 16%)	32 (31, 65%)	48 (33, 54%)

Table 5. Global aerosol budgets in ModelE2-OMA. Note that the sulfate and nitrate budgets are presented as Tg S and Tg N, respectively.

	Sulfate	EC	OM	Sea-salt	Dust	Nitrate
Burden [Tg]	0.38	0.12	1.1	9.3	11.4	0.37
Total source [Tg yr-1]	52.0	7.4	58.5	2866.7	1071.8	21.0
Emission	1.7	7.4	43.7	2866.7	1071.8	
Wet deposition [Tg yr-1]	46.6	5.4	44.9	2059.1	407.7	17.7
By convective clouds [%]	21	37	32	39	52	29
Dry deposition [Tg yr-1]	5.4	2.0	13.7	806.9	664.1	3.3
Lifetime [days]	2.6	5.8	7.1	1.2	3.9	6.4
Removal rate coefficient [day-1]	0.39	0.17	0.14	0.84	0.26	0.16
Wet deposition	0.35	0.13	0.11	0.61	0.10	0.13
Dry deposition	0.04	0.046	0.033	0.24	0.16	0.025
Wet/(Wet+Dry) [%]	90	73	77	72	38	84

Table 6. Statistical measures of model predictions compared to satellites. For ModelE2-OMA, the model prediction without nitrate aerosols is also presented in parentheses.

		Model vs. MODIS	Model vs. MISR	MODIS vs. MISR
ModelE2-TOMAS	Correlation	0.63	0.73	0.79
	NMB [%]	-29%	-34%	8%
ModelE2-OMA	Correlation	0.45 (0.45)	0.52 (0.55)	0.79
	NMB [%]	16% (-16%)	8% (-21%)	8%

Table 7. Locations of AERONET sites and corresponding measurement time periods.

	Sites	Longitude	Latitude	Years
1	Alta Floresta	56.0° W	9.9° S	1999-2005
2	Abracos Hill	62.0° W	11° S	1999-2005
3	Cuiaba-Miranda	56.0° W	15.7° S	2001-2005
4	Mongu	23.2° E	15.2° S	1995-2005
5	Ilorin	4.3° E	8.3° N	1998-2005
6	Banizombou	2.0° E	13.0° N	1995-2005
7	Capo Verde	22.9° W	16.7° N	1994-2004
8	Bidi Bahn	2.5° W	14.1° N	1996-1997
9	Barbados	59.5° W	13.2° N	1996-2000
10	Sede Boker	34.8° E	30.9° N	1998-2005
11	Bahrain	50.6° E	26.2° N	2004-2005
12	Solar Village	46.4° E	24.9° N	1999-2005
13	Dalanzadgad	104.4° E	43.6° N	1997-2005
14	Yulin	109.7° E	38.3° N	2001-2002
15	Sevilleta	106.9° W	34.4° N	1994-2005
16	Cart site	97.5° W	36.6° N	1996-2005
17	Bondville	88.4° W	40.1° N	1996-2005
18	GSFC	76.8° W	39.0° N	1995-2005
19	Mexico city	99.2° W	19.3° N	1999-2005
20	Ispra	8.6° E	45.8° N	2001-2005
21	Kanpur	80.3° E	26.5° N	2001-2005
22	Shirahama	135.4° E	33.7° N	2000-2005
23	Bermuda	64.7° W	32.4° N	1996-2005
24	Lanai	156.9° W	20.7° N	1996-2004
25	Dry Tortugas	82.9° W	24.6° N	1996-2003
26	Tahiti	149.6° W	17.6° S	1999-2005
27	Rottnest Island	115.5° E	32.0° N	2001-2004
28	Nauru	166.9° E	0.5° S	1999-2005

Table 8. Summary of global annual-average of tropospheric and surface-layer aerosol number budgets including J3 (new particle formation rates at 3 nm), CN3 (number concentration of particles with Dp ≥ 3 nm), CN10(Dp ≥ 10 nm), CN100(Dp ≥ 100 nm) in ModelE2-TOMAS. Values normalized by tropospheric volume at 273 K and 1 atm.

	Emission rate [cm^{-3} s^{-1}]	Tropospheric J3 [cm^{-3} s^{-1}]	Tropospheric CN3 [cm^{-3}]	Tropospheric CN10 [cm^{-3}]	Tropospheric CN100 [cm^{-3}]	Surface-layer CN3 [cm^{-3}]	Surface-layer CN10 [cm^{-3}]	Surface-layer CN100 [cm^{-3}]
Base	5.47×10^{-4}	0.131	4852	939	211	1622	1331	416
LowNUC	5.47×10^{-4}	0.013	1277	628	197	1152	1111	405
NoNUC	5.47×10^{-4}	0.000	222	221	159	935	919	374

Figure 1. Annual-average column mass concentrations of (a) DMS and (b) SO_2 in the ModelE2-TOMAS BASE run. Units are μg S m^{-2}.

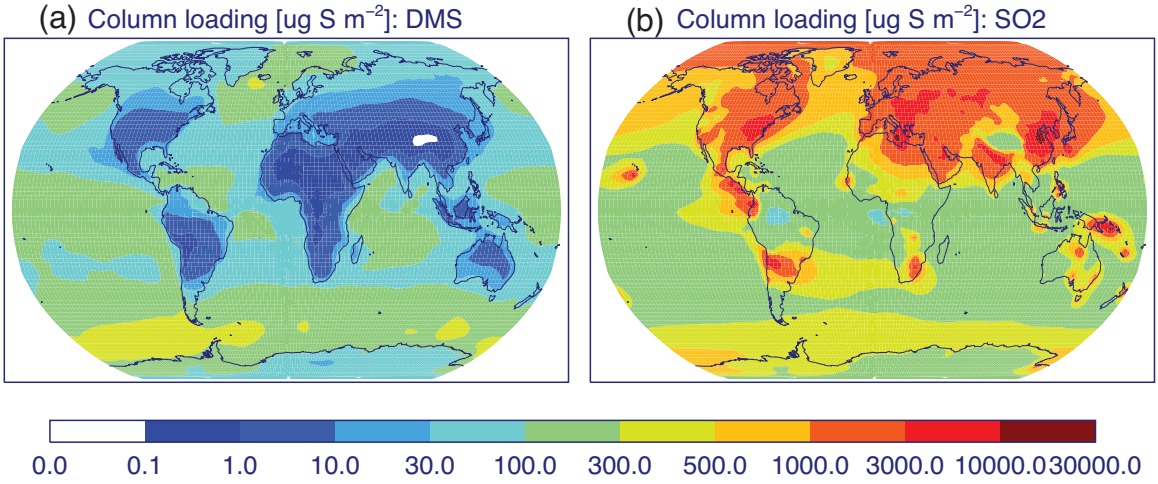

Figure 2. Scatter plot of annual-mean surface SO_2 concentrations [μg m^{-3}] for the model (red for ModelE2-TOMAS and blue for ModelE2-OMA) compared to the observations in the EMEP (European Monitoring and Evaluation Programme, Loevblad et al., 2004; a) and CASTNET (Clean Air Status and Trends Network, Malm et al., 2002; b) networks. Log-mean normalized bias (LMNB) and log-mean normalized error (LMNE) are given.

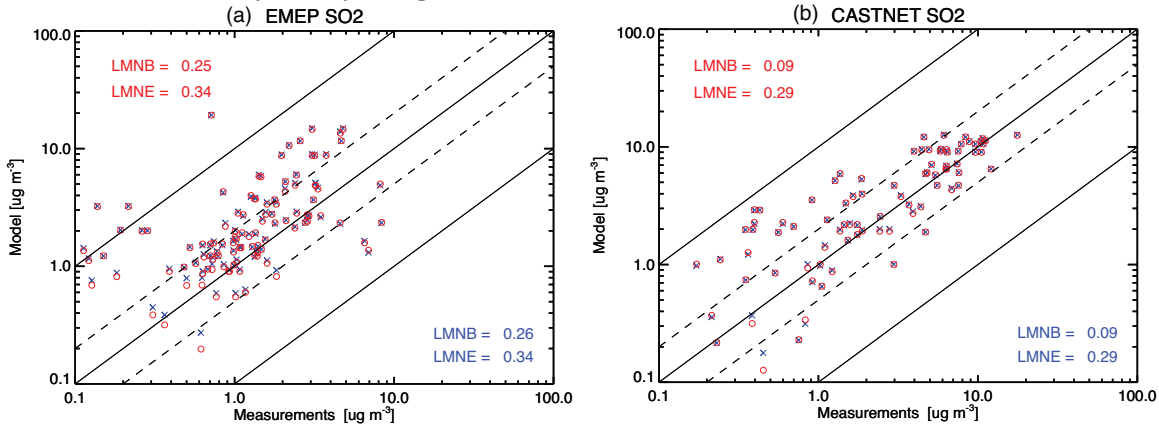

Figure 3. Comparisons of monthly averaged surface DMS (a to c) and SO_2 (d to e) mixing ratios [pptv] simulated (red for ModelE2-TOMAS and blue for ModelE2-OMA) and measured (black) at Amsterdam Island [Nguyen et al., 1992] and Cape Grim [Ayers et al., 1991]. Only DMS at Dumont D'Urville [Jourdain and Legrand, 2001]. Correlation (R) and normalized mean bias (NMB) are given.

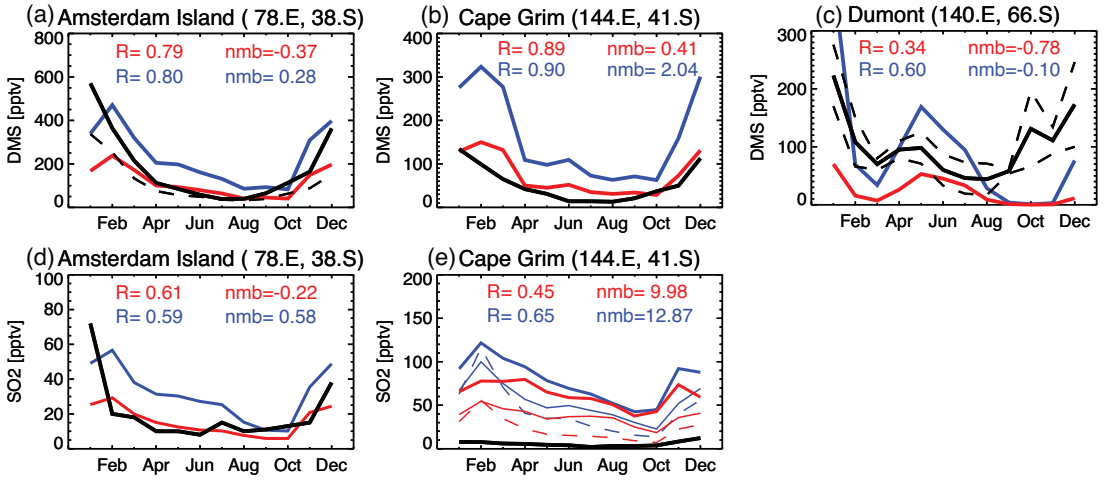

Figure 4. Comparison of DMS vertical profiles over the Pacific Ocean simulated (red for ModelE2-TOMAS and blue for ModelE2-OMA) and observed (black solid line). Observations are from PEM-Tropic-A (August-October 1996 in the tropical Pacific; Christmas Island in a; Hawaii in c; Tahiti in e; Easter Island in g; Fiji in h) and PEM-Tropic-B (March-April 1999 in the tropical Pacific; Christmas Island in b; Hawaii in d; Tahiti in f). The dashed lines represent 25th and 75th percentiles of the observed values.

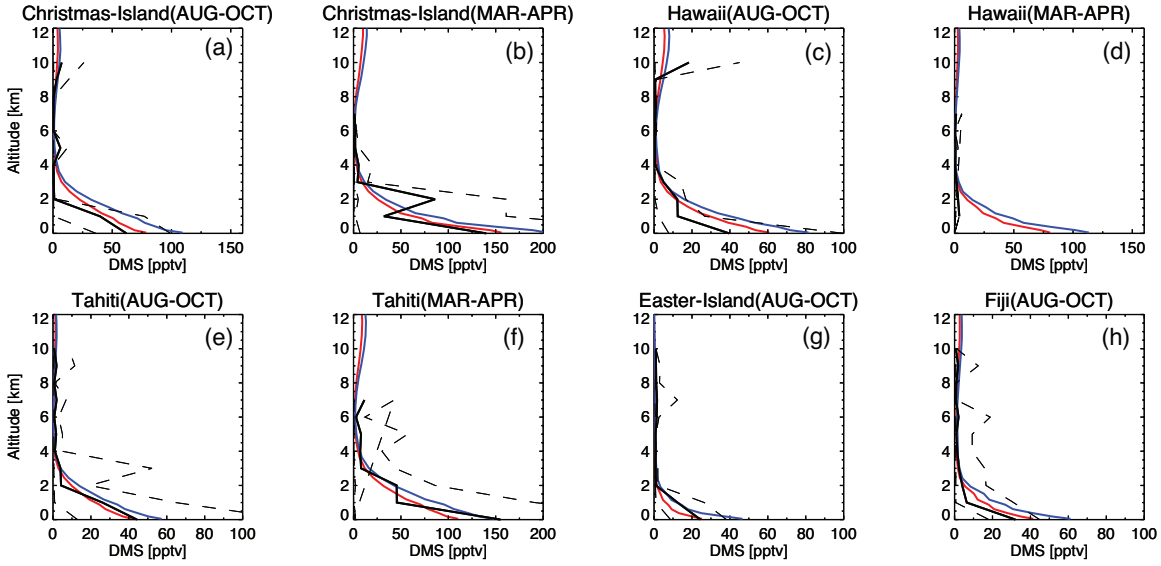

Figure 5. The same as Fig. 4 but for SO_2 vertical profiles.

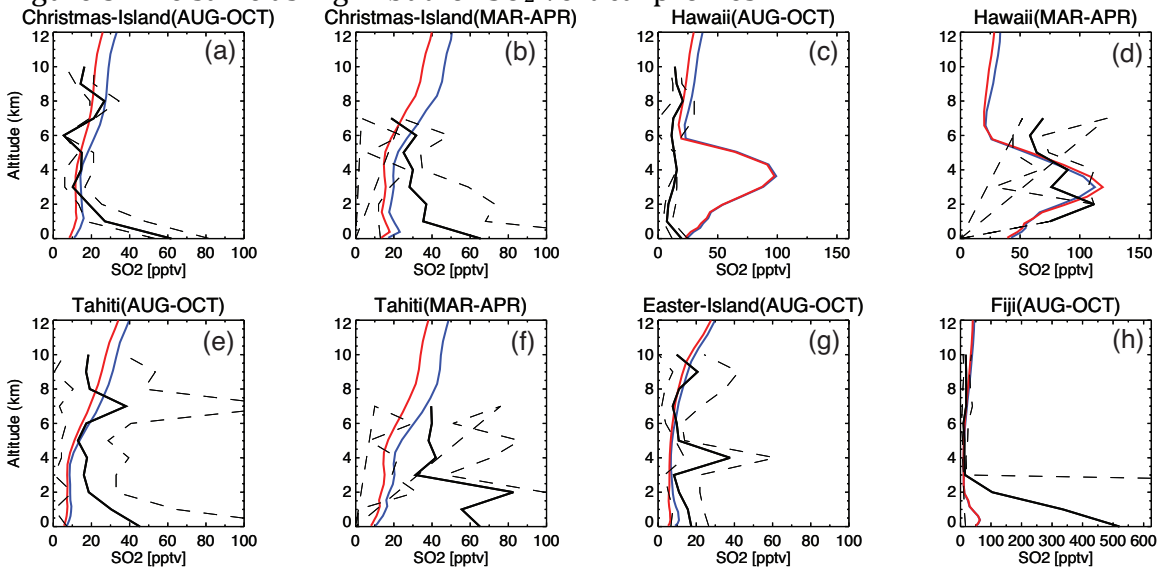

Figure 6. Annual-mean concentrations of (a) sulfate, (b) EC, (c) OM, (d) sea-salt, and (e) dust in the lowermost layer in the ModelE2-TOMAS BASE run. Units are μg m^{-3}.

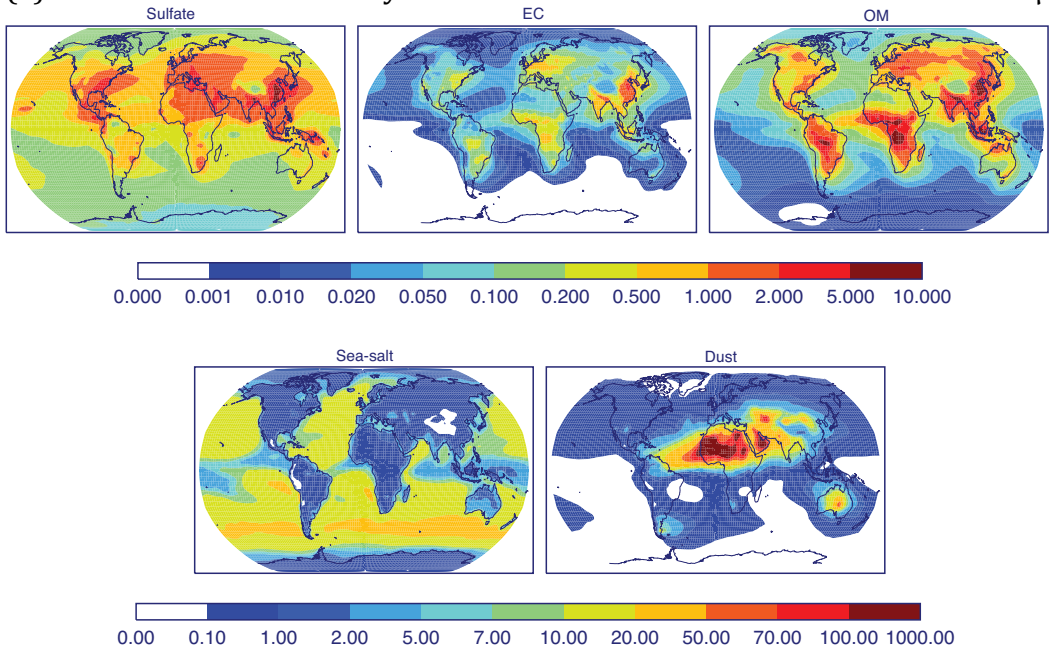

Figure 7. Annually and zonally averaged concentrations of (a) sulfate, (b) EC, (c) OM, (d) sea-salt, and (e) dust in the ModelE2-TOMAS BASE run. Units are μg m^{-3}.

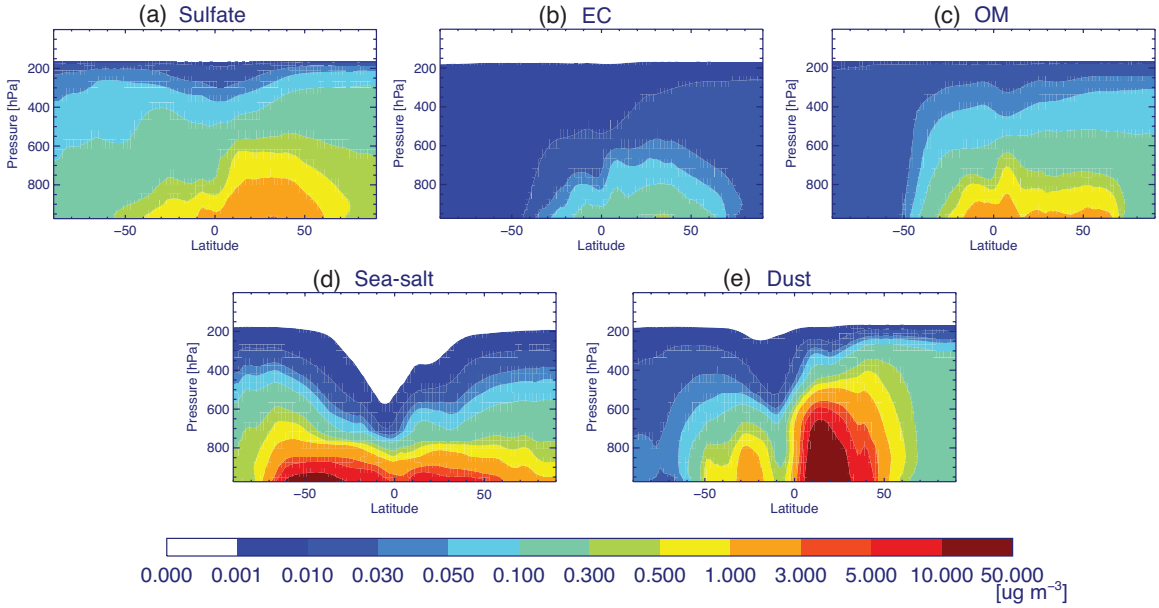

Figure 8. Scatter plot of annually averaged surface sulfate mass concentrations [μg m^{-3}] in the model (red for ModelE2-TOMAS and blue for ModelE2-OMA) and observation from (a) the IMPROVE network, (b) the European sites from Putaud et al. (2010), and (c) University of Miami. Note that the sulfate in the model is simply converted to ammonium sulfate at the IMPROVE sites.

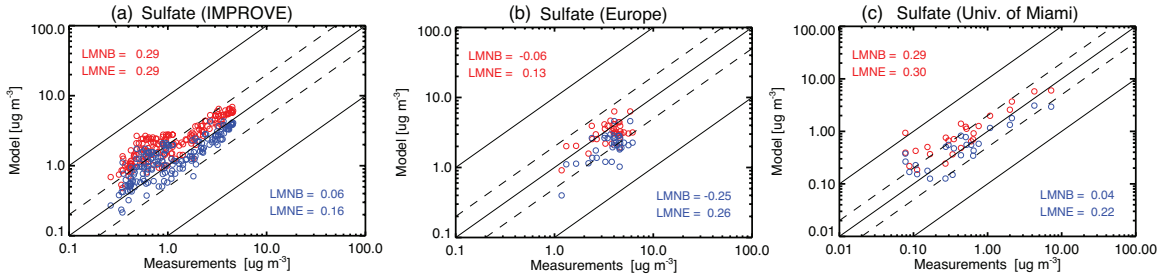

Figure 9. Comparisons of monthly averaged surface sulfate mass concentrations [μg m^{-3}] simulated (red for ModelE2-TOMAS and blue for ModelE2-OMA) and measured (black solid line with an error bar showing a standard deviation) by University of Miami. Correlation (R) and normalized mean bias (NMB) are provided only when the observation is available for 12 months.

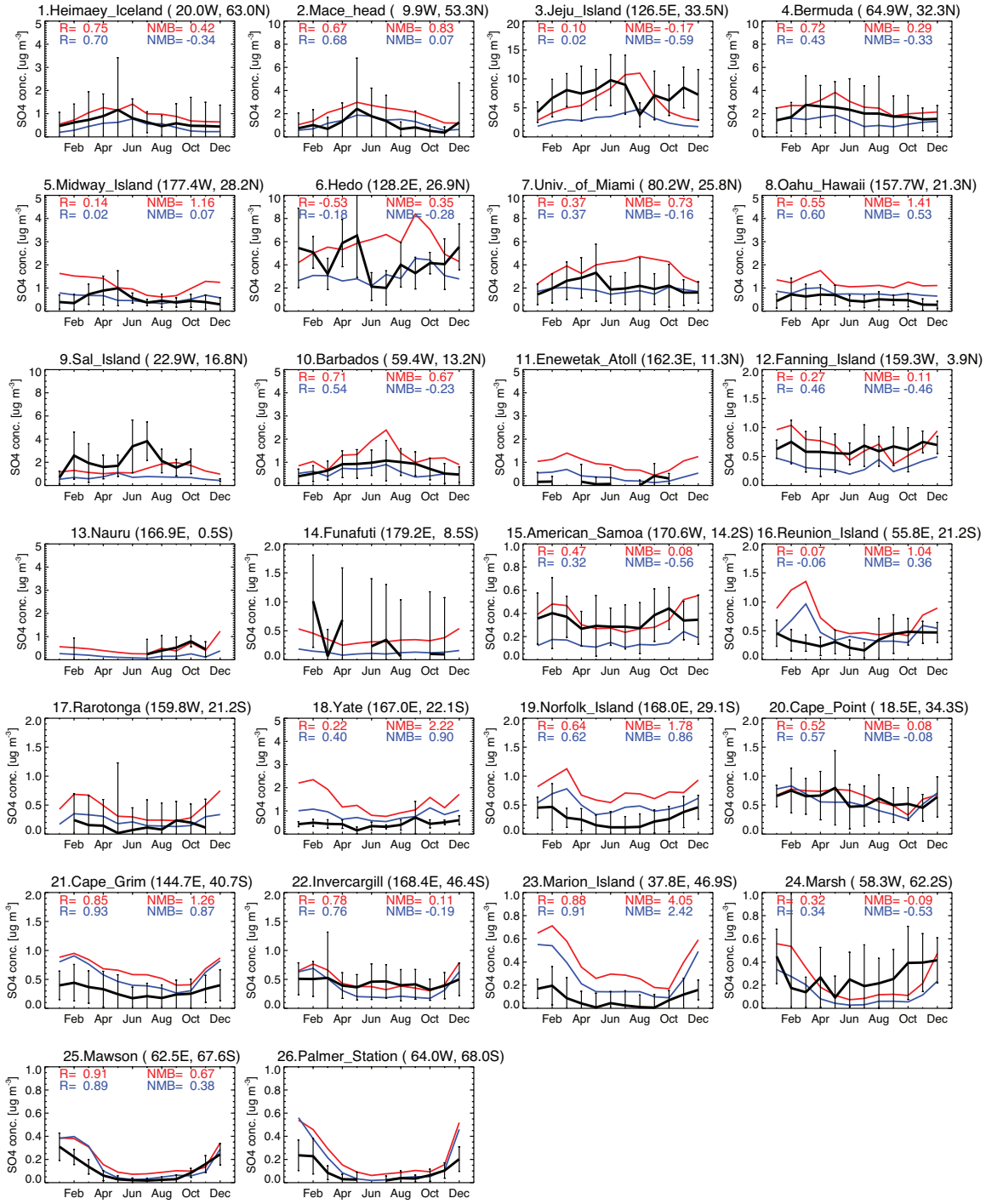

Figure 10. Same as Figure 8 but for sea-salt mass concentrations

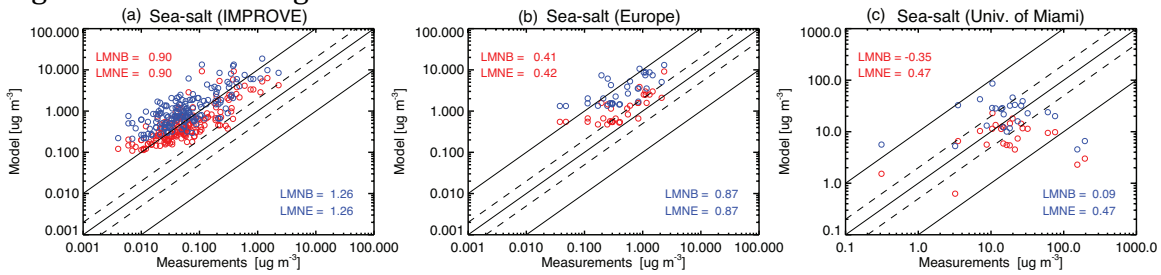

Figure 11. Same as Figure 9 but for sea-salt mass concentrations

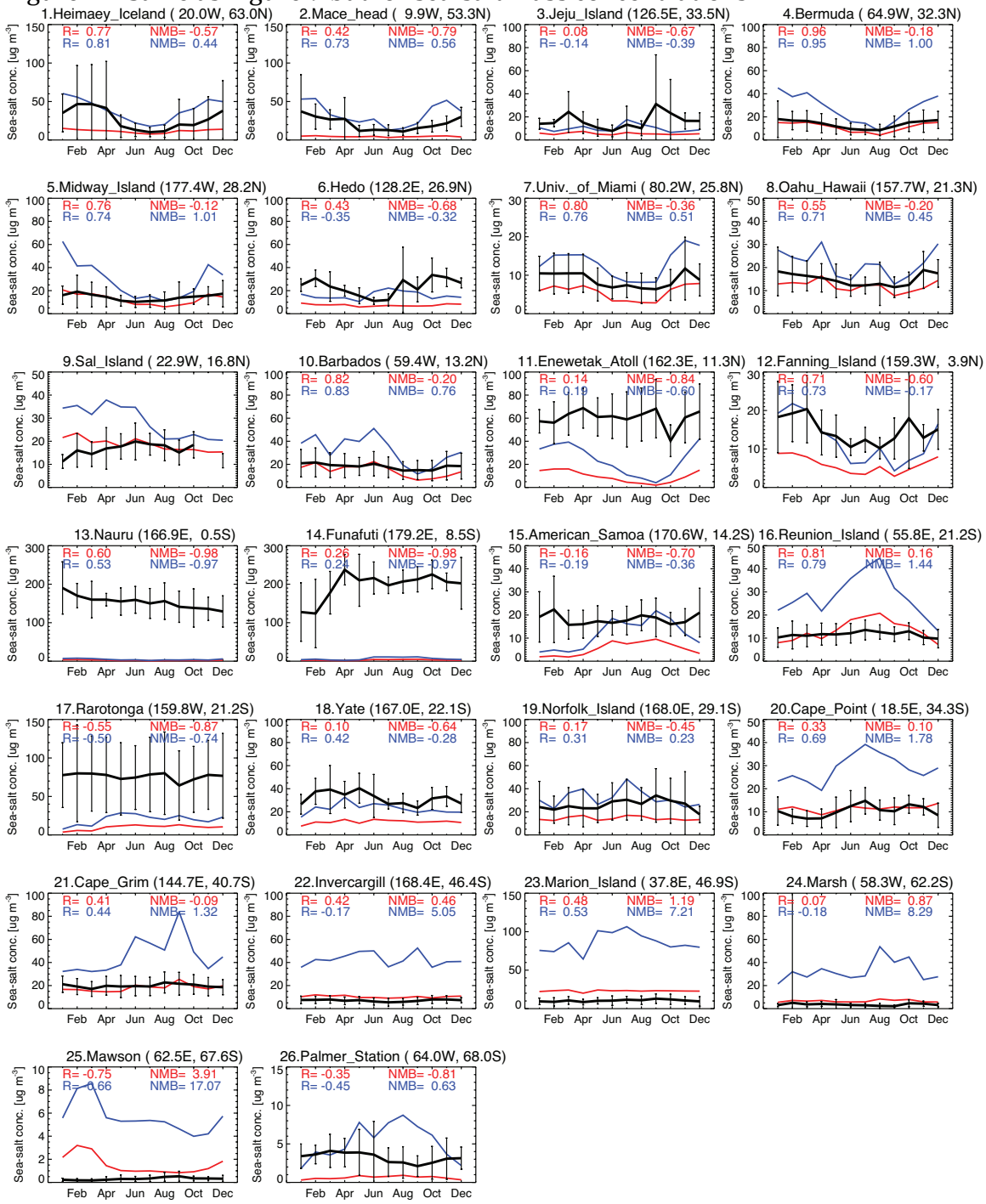

Figure 12. Same as Figure 8 but for dust mass concentrations

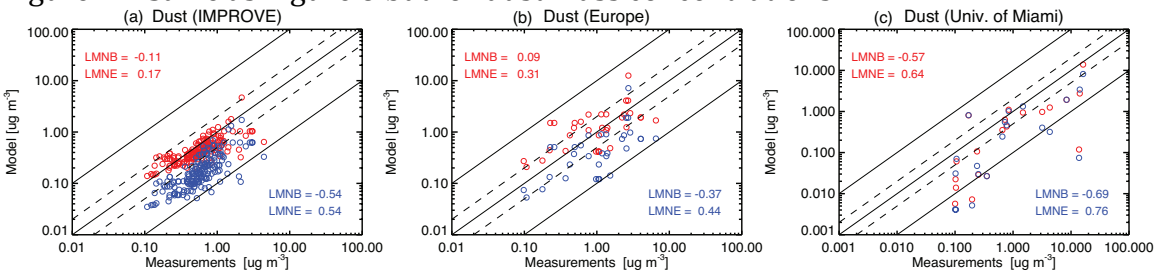

Figure 13. Same as Figure 9 but for dust mass concentrations

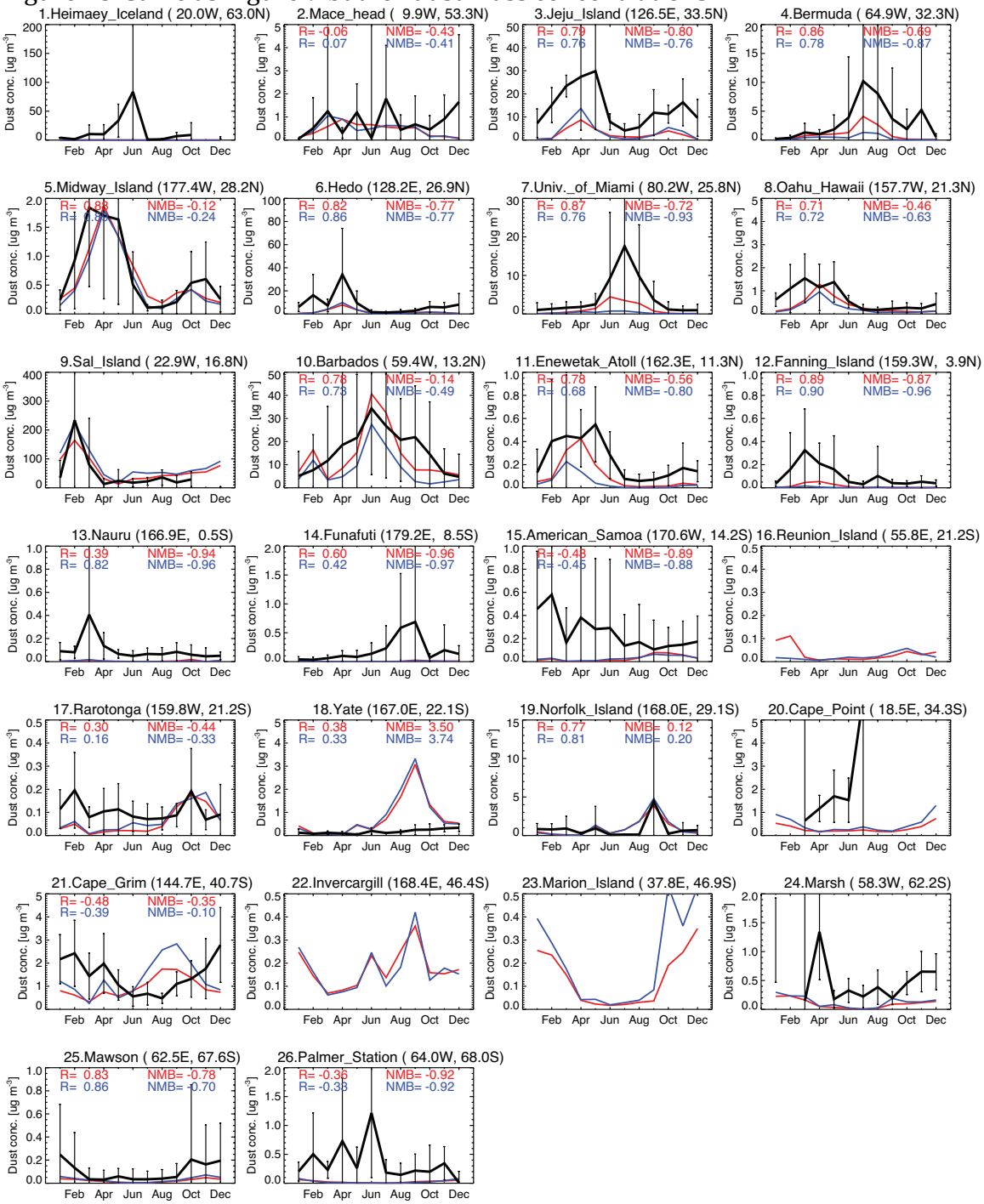

Figure 14. Scatter plot of annual-average dust deposition fluxes [mg m^{-2} yr^{-1}] simulated and observations obtained from Ginoux et al. (2001), Tegen et al. (2002) and Tables S2 in Mahowald et al. (2009). Open symbols are for ModelE2-TOMAS and the filled symbol for ModelE2-OMA. LMNB and LMNE are presented below the plot: the first values are for ModelE2-TOMAS.

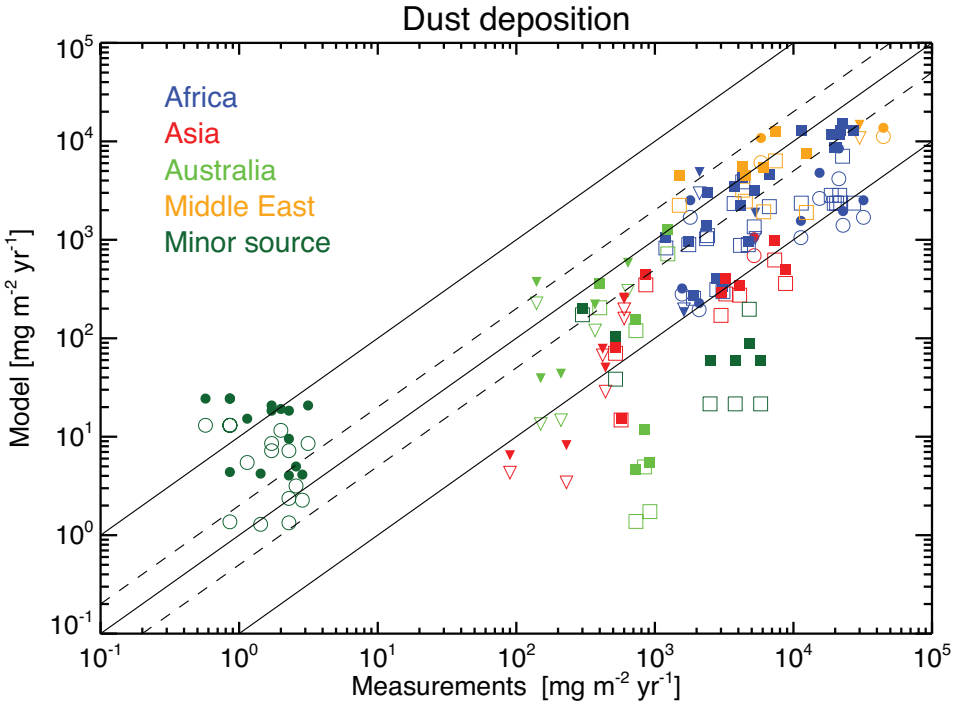

Mahowald et al.[2009] - o	Ginoux et al.[2001] - v	Tegen et al.[2002] - sq
LMNB = -0.04	LMNB = -0.77	LMNB = -0.90
LMNE = 0.68	LMNE = 0.81	LMNE = 0.91
LMNB = 0.24	LMNB = -0.54	LMNB = -0.61
LMNE = 0.82	LMNE = 0.64	LMNE = 0.65

Figure 15. Scatter plots of annually averaged surface EC and OM mass concentrations [μg m^{-3}] simulated (red for ModelE2-TOMAS and blue for ModelE2-OMA) and observations from the IMPROVE network (a and b) and the European sites from Putaud et al. (2010) (c and d).

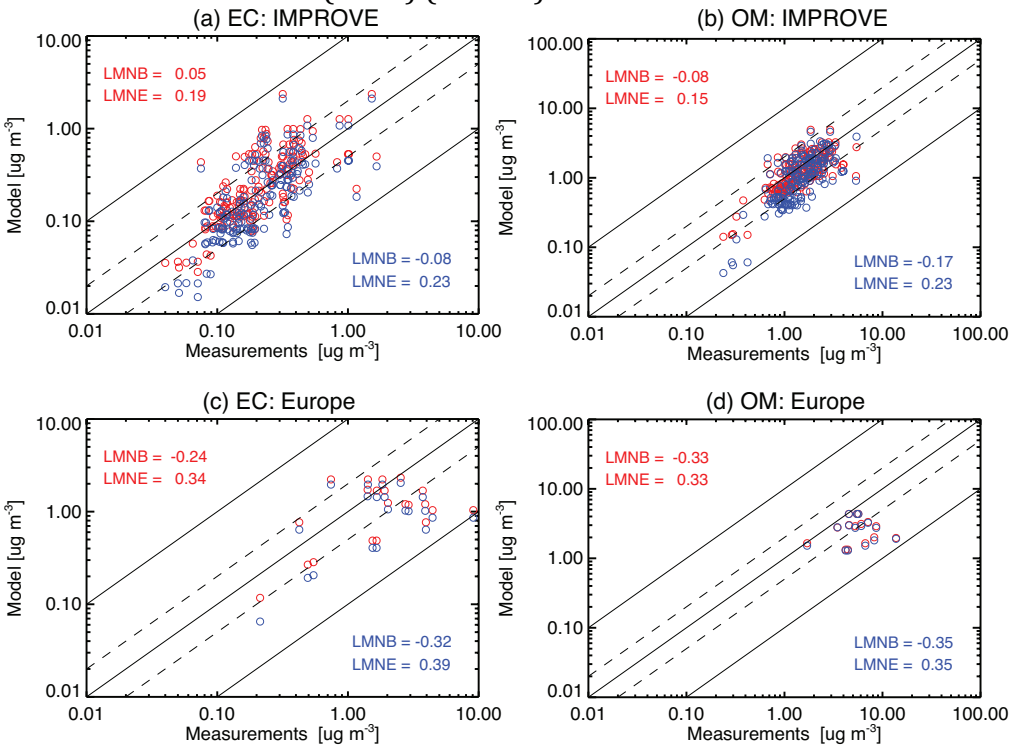

Figure 16. Scatter plots of annually averaged surface PM2.5 concentration [μg m^{-3}] simulated and observations compiled by the Global Burden of Disease (GBD) Study. ModelE2-TOMAS is shown in (a) and ModelE2-OMA in (b).

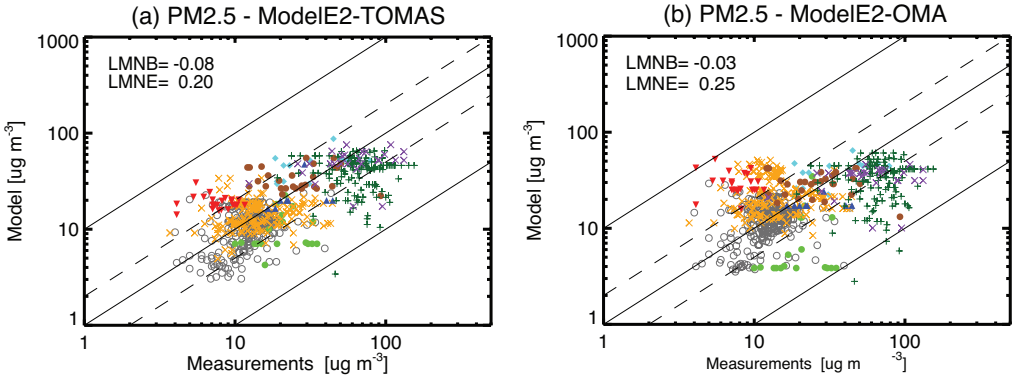

Figure 17. Global distributions of the annual-mean AOD from (a) ModelE2-TOMAS, (b) ModelE2-OMA, (c) MISR, and (d) MODIS. See Section 5.4 for the details of the MISR and MODIS AOD information.

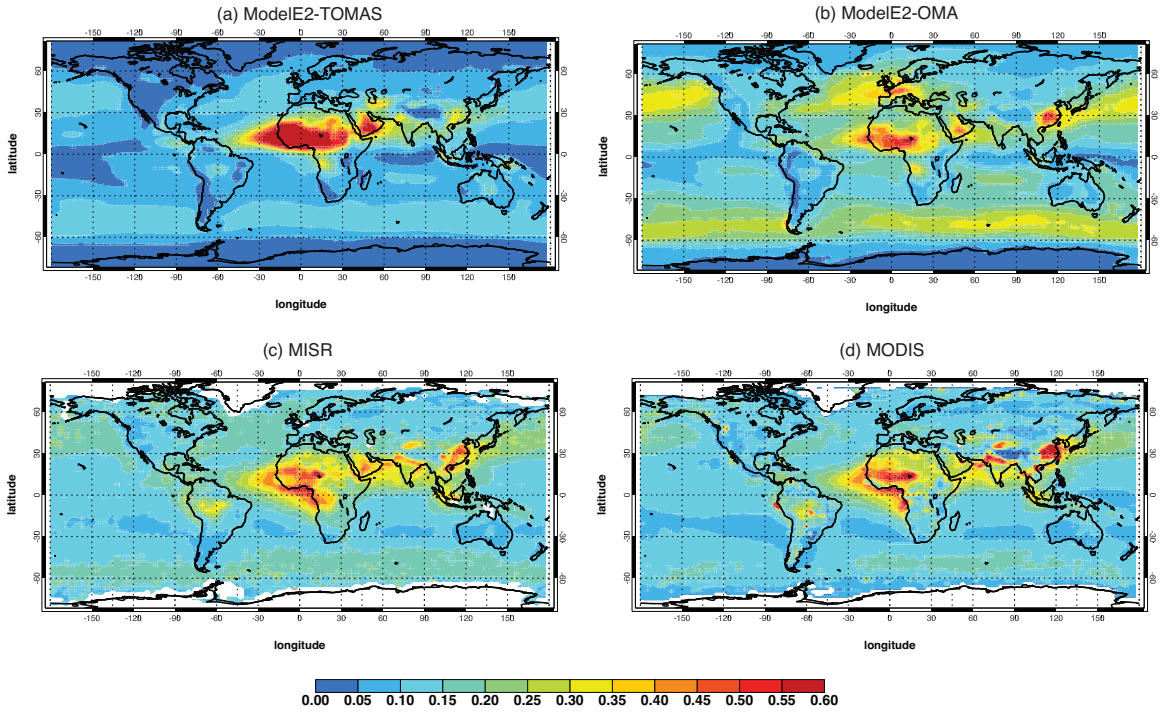

Figure 18. Comparisons of monthly averaged model AOD (red for ModelE2-TOMAS and blue for ModelE2-OMA) and AERONET AOD (black solid line). Correlation (R) and normalized mean bias (nmb) are provided only when the observation is available for 12 months.

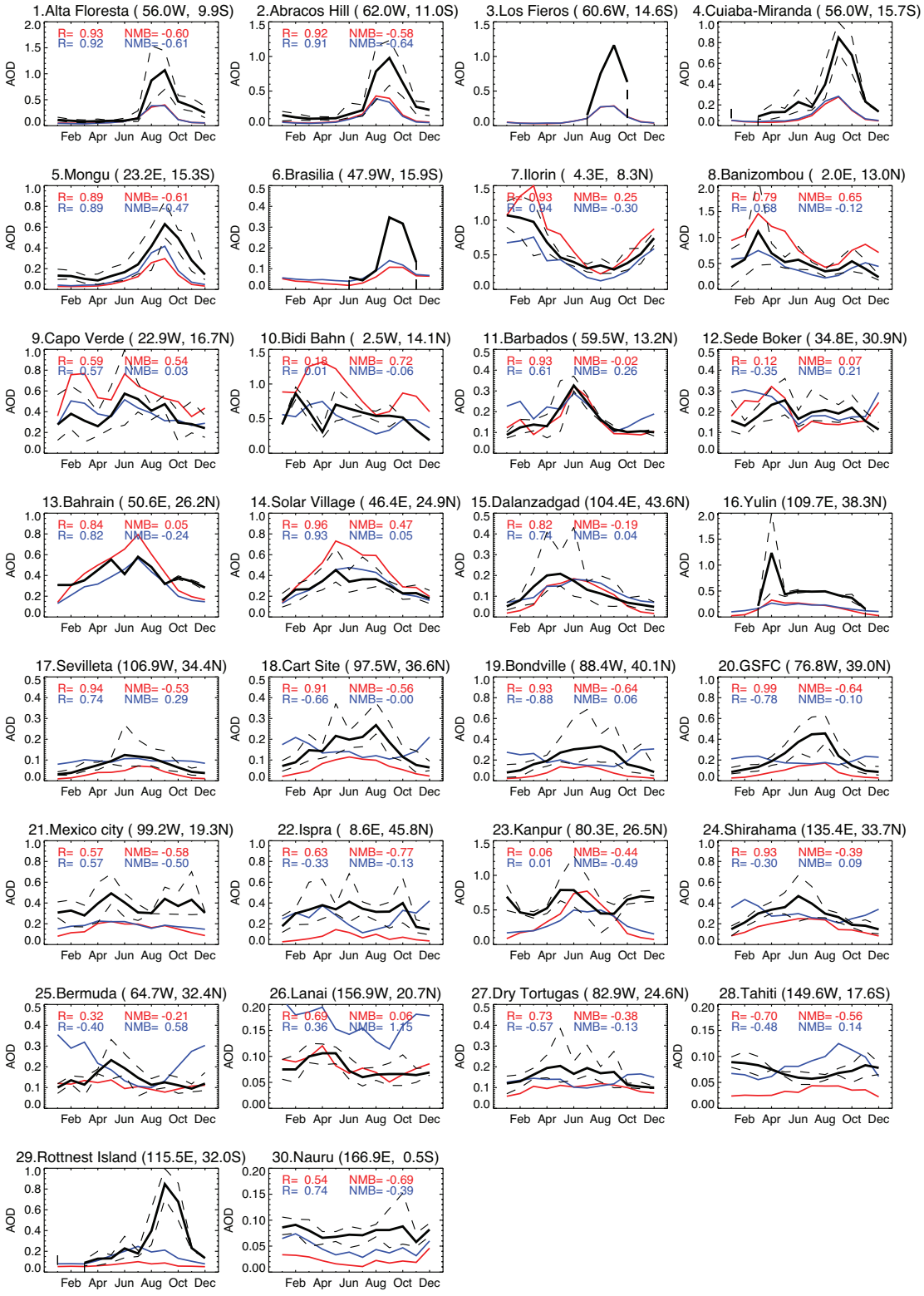

Figure 19. Annually averaged CN3 ($D_p \geq 3$ nm), CN10 ($D_p \geq 10$ nm), CN100 ($D_p \geq 100$ nm) concentrations in the lowermost layer for the BASE run (a to c), the LowNUC run (d to f), and the NoNUC run (g to i) of ModelE2-TOMAS. Units are cm^{-3}.

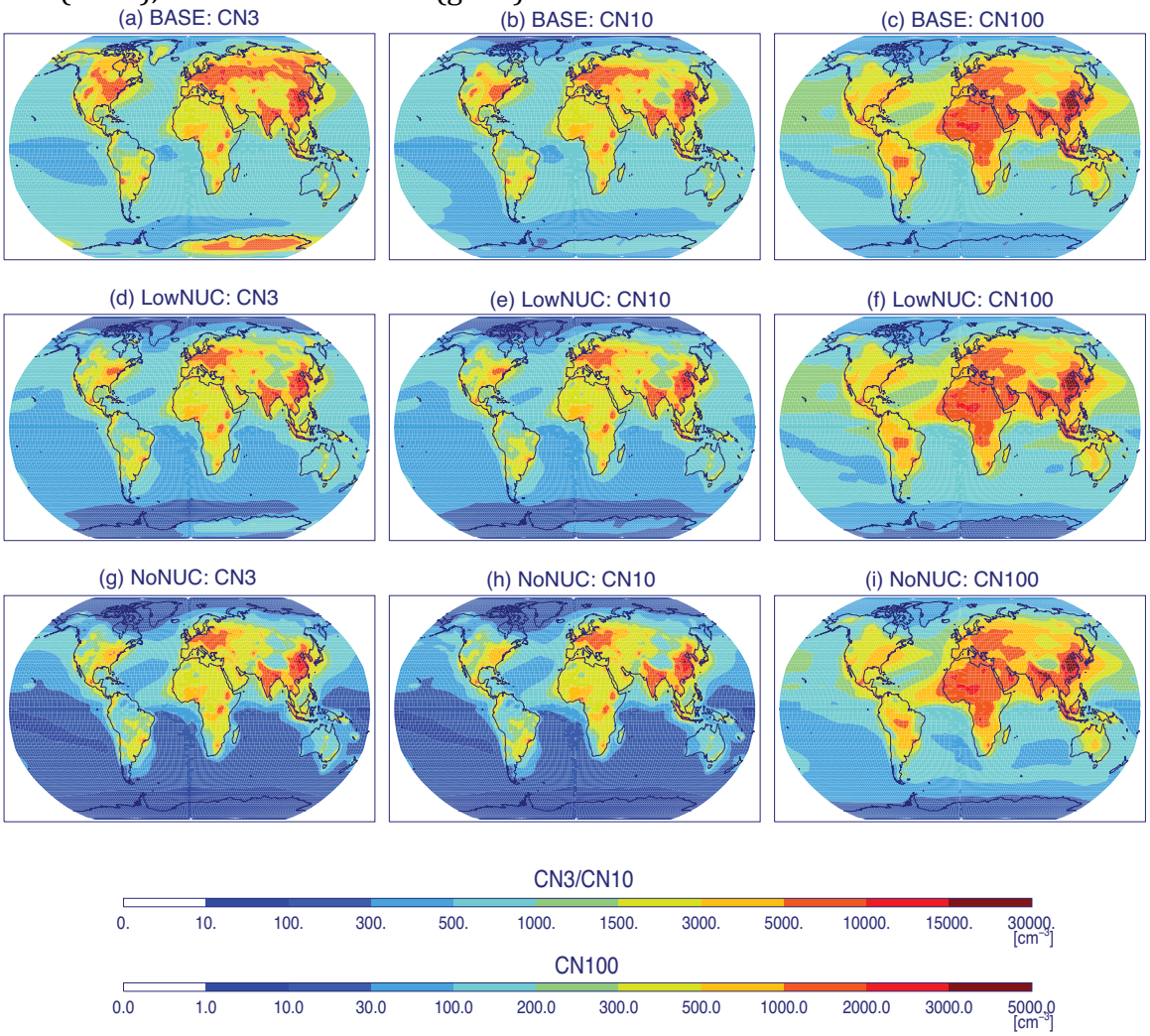

Figure 20. Annually and zonally averaged CN3 (Dp ≥ 3 nm), CN10(Dp ≥ 10 nm), and CN100(Dp ≥ 100 nm) concentrations for the BASE run (a to c), the LowNUC run (d to f), and the NoNUC run (g to i) of ModelE2-TOMAS. Units are cm^{-3}.

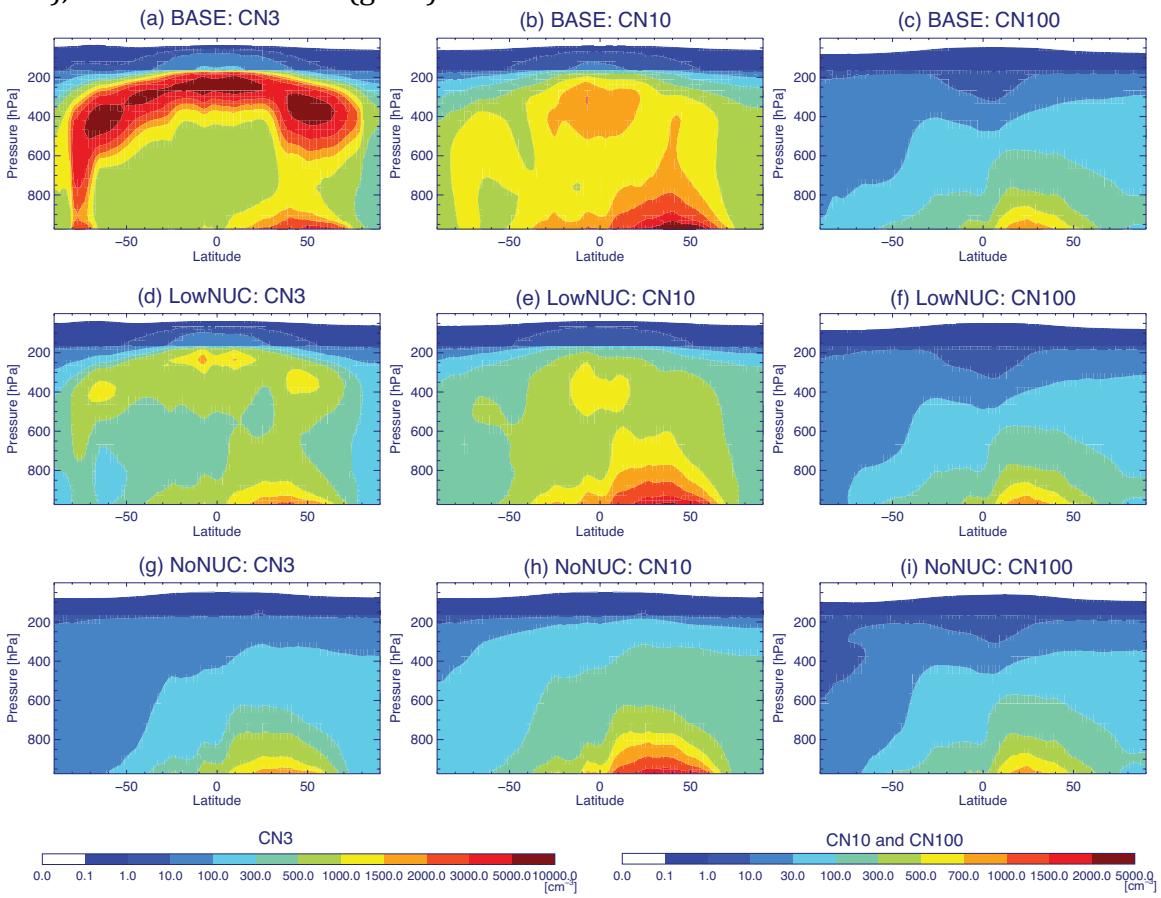

Figure 21. Scatter plot of simulated annual-mean aerosol number concentrations in comparison with a dataset of surface number concentrations measurements at 36 sites around the world compiled by Spracklen et al. (2010). The top horizontal bar represents the BASE results, and the middle bar the LowNUC results and the lower bar the NoNUC results. Red color is for free troposphere (FT); blue for marine boundary layer (MBL); green for continental boundary layer (CBL).

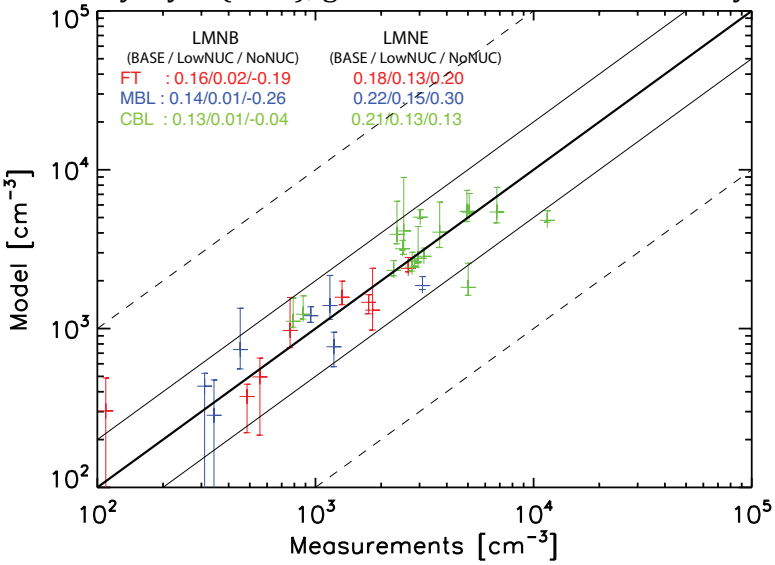

Figure 22. Annual cycle of aerosol number concentrations [cm^{-3} at ambient conditions] at 32 sites. The observations are shown in black, and three model results are presented: red for BASE, blue for LowNUC, and green for NoNUC. The free tropospheric (FT) sites are from 1 to 8; the marine boundary layer (MBL) sites, 9 to 15; the continental boundary layer (CBL) sites,16 to 32. Correlation (R) and normalized mean bias (NMB) are provided only when the observation is available for 12 months.

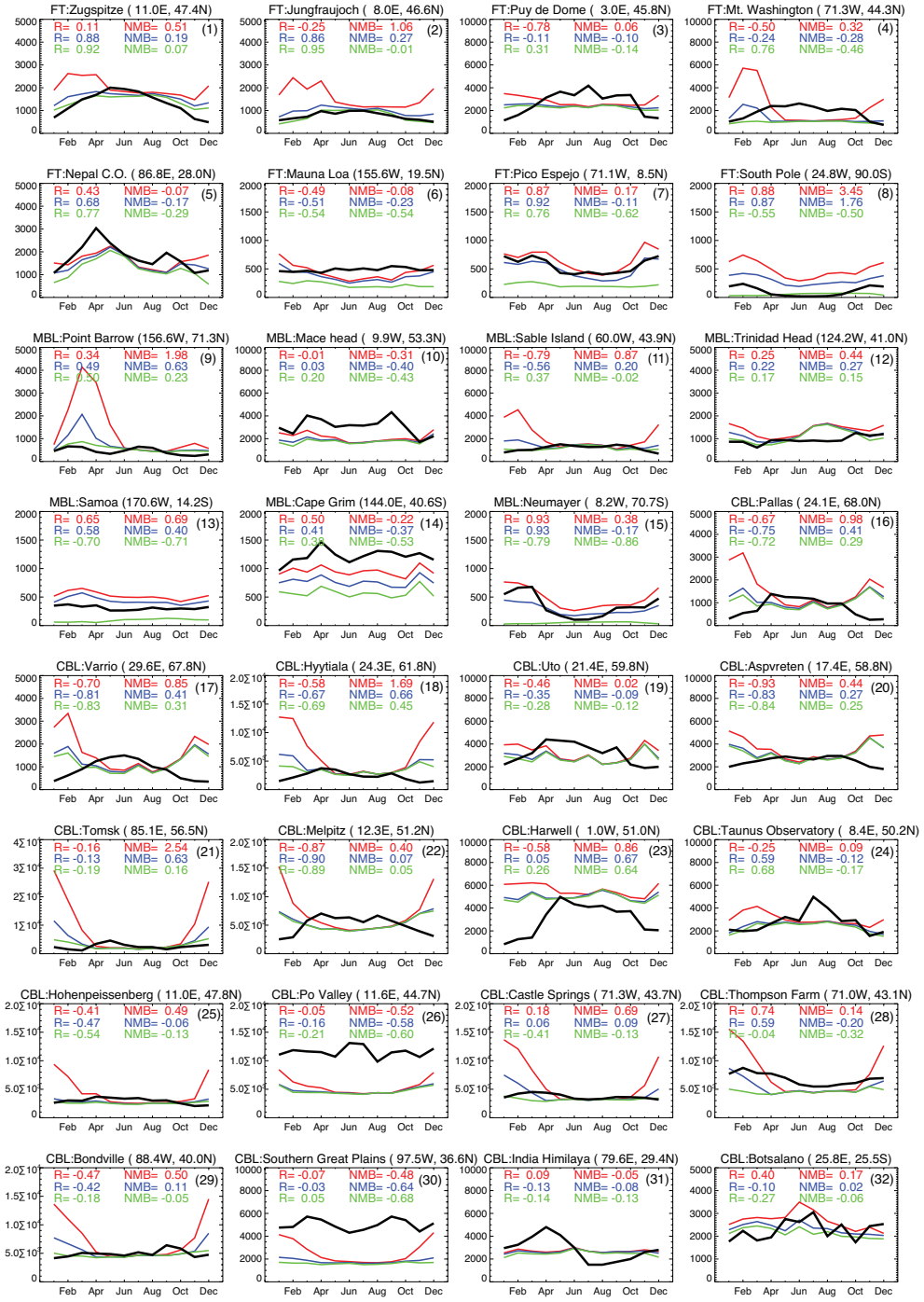

Figure 23. Number size distributions from European sites during winter (DJF; a to f) and summer (JJA; g to l) that are obtained from log-normal 3-mode fits during morning (black solid), afternoon (black dotted), and night (black dashed). The model results are the seasonal mean, shown in red lines for the BASE run, blue lines for the LowNUC run, and green lines for the NoNUC run.

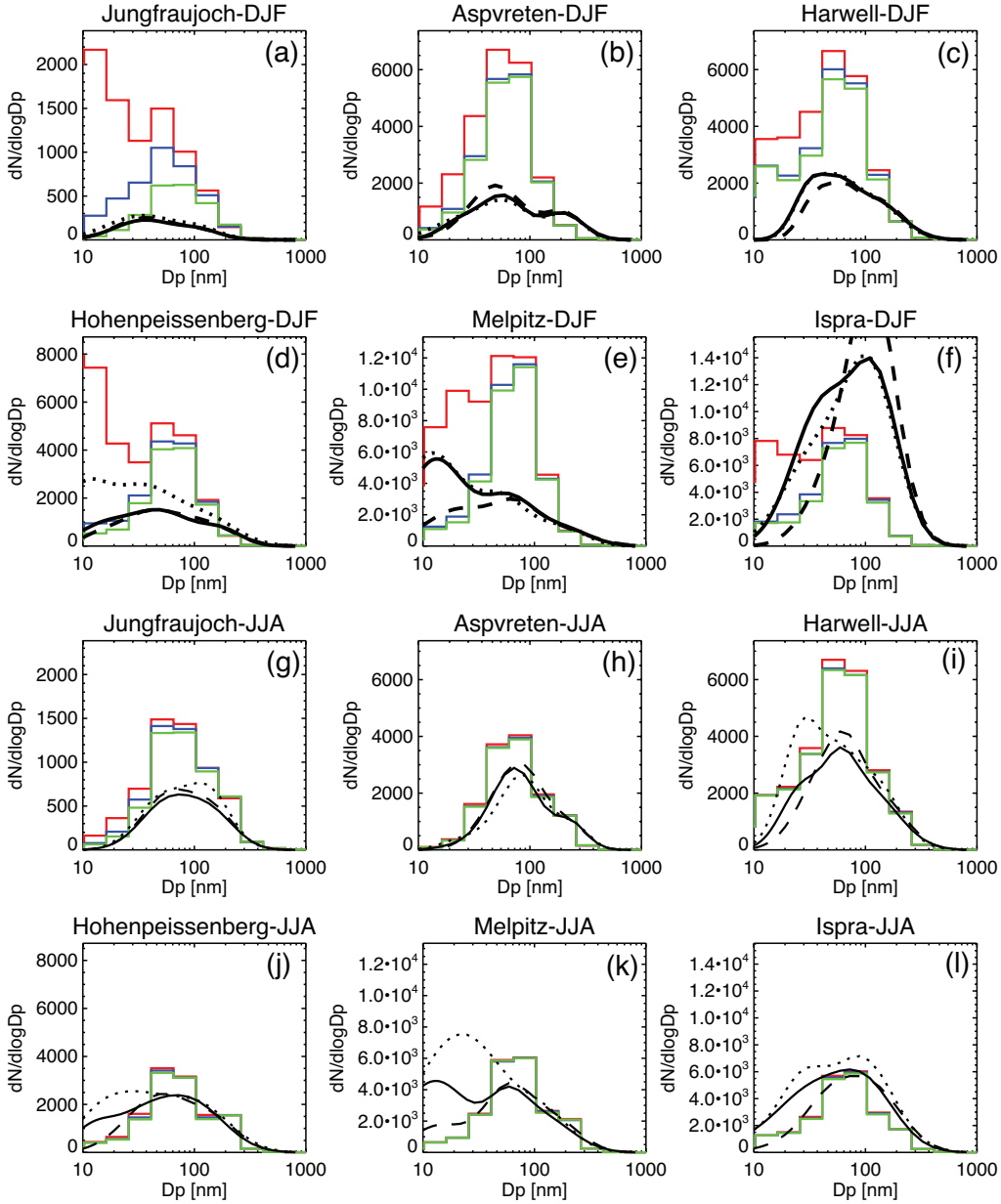

Figure 24. Vertical profiles of aerosol number concentrations from the observations (black lines) and ModelE2-TOMAS (red lines for the BASE run, blue lines for the LowNUC run, and green lines for the NoNUC run). The CN5, CN15, CN120 concentrations (ambient conditions) from LACE campaign (Petzold et al., 2002, in north-east Germany) are shown in a to c, respectively. The observed CN3 concentrations (STP conditions: 1atm, 273 K) over the Pacific Ocean, which are averaged into the 3 latitude bands (70 S to 20S, 20S to 20N, and 20N to 70N; Clarke and Kapustin, 2002), are shown in d to f. The dashed lines show the standard deviation for the observations and the min/max monthly mean for the model (only in d to f).

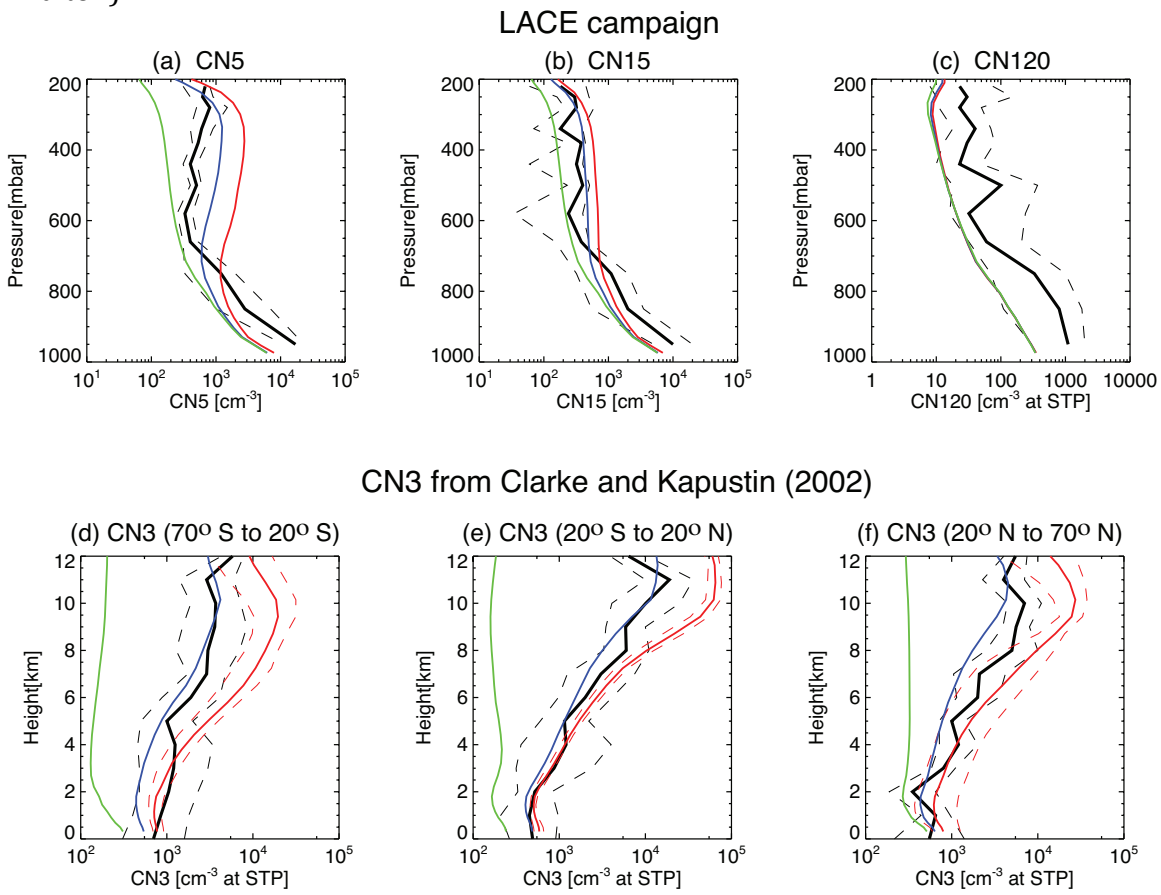

Figure 25. Simulated number concentrations in (a) Aitken mode (10 nm ≤ Dp < 100 nm) and (b) accumulation mode (100 nm ≤ Dp < 1 μm) compared to the observations ("x" symbol with error bar representing minimum and maximum observed concentrations) that were compiled and aggregated into 15-degree latitude ranges (Heintzenberg et al. 2002). The model is also averaged to the 15-degree grid and is shown in red lines for the BASE run, blue lines for the LowNUC run, and green lines for the NoNUC run.

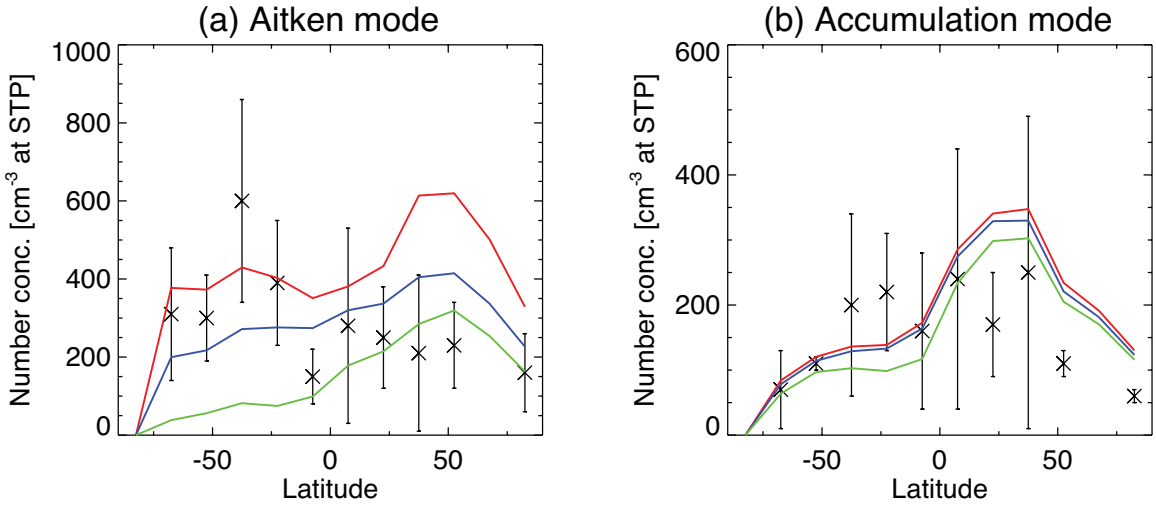

Figure 26. Annually and zonally averaged aerosol size distributions in the marine boundary layer. Observations are from Heintzenberg et al. (2000) and were compiled and aggregated into a 15° x 15° grid. The model is also averaged to the 15-degree grid and is shown as red lines for the BASE run, blue lines for the LowNUC run, and green lines for the NoNUC run.

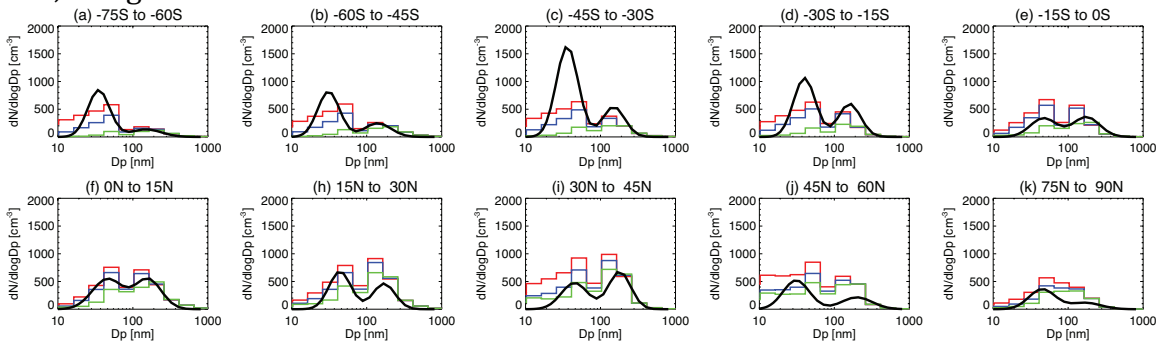

Figure 27. Scatter plot of simulated CCN concentrations in comparison with a dataset of CCN measurements compiled by Spracklen et al. (2011). Data is classified into two categories: CCN in the MBL (in black) and CCN in the CBL (in red). The upper error bar is for the BASE run, the middle symbol for the LowNUC run, and the lower error bar for the NoNUC run. Large and filled symbols are for measurement duration longer than 10 days, and small and open symbols for less than 10 days. Circle symbols are for supersaturations (*s*) less than 0.2%; upward triangles for *s* greater than 0.2% and less than 0.8%; downward triangle for *s* greater than 0.8%.

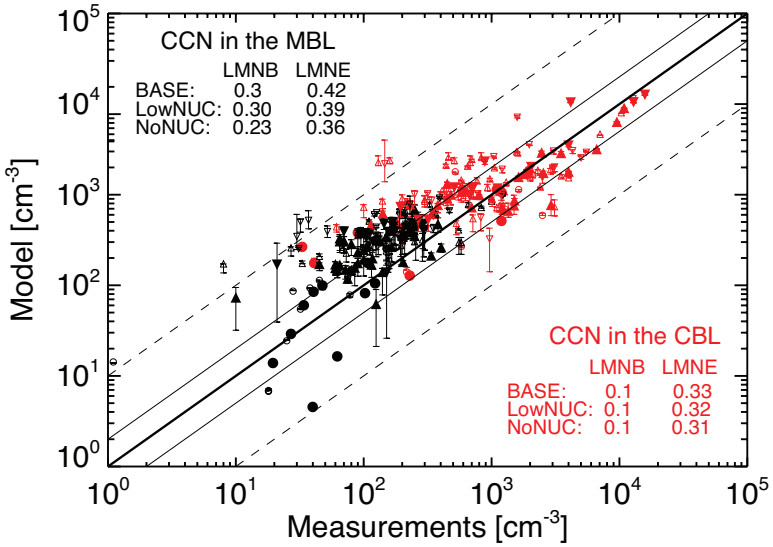

Figure 28. Annual cycle of CCN concentrations at Cape Grim (supersaturations (*s*) of 1.2% in a, 0.75% in b, and 0.23% in c) and Mace Head (*s* of 0.5% in d). The measured CCN concentrations are shown in black, and the simulated CCN in red for the BASE run, blue for the LowNUC run, and green for the NoNUC run. Correlation (R) and normalized mean bias (NMB) are given.